ACS Catalysis

Research Article

Cite This: ACS Catal. 2019, 9, 6234−6242

pubs.acs.org/acscatalysis

Modulating Fatty Acid Epoxidation vs Hydroxylation in a Fungal Peroxygenase

Juan Carro,[†,⊥] Alejandro González-Benjumea,[‡,⊥] Elena Fernández-Fueyo,[†,⊥,#] Carmen Aranda,[‡] Victor Guallar,[*,§,∥] Ana Gutiérrez,[*,‡] and Angel T. Martínez[*,†]

[†]Centro de Investigaciones Biológicas, CSIC, Ramiro de Maeztu 9, E-28040 Madrid, Spain

[‡]Instituto de Recursos Naturales y Agrobiología, CSIC, Reina Mercedes 10, E-41012 Sevilla, Spain

[§]Barcelona Supercomputing Center, Jordi Girona 29, E-08034 Barcelona, Spain

[∥]ICREA, Passeig Lluís Companys 23, E-08010 Barcelona, Spain

Supporting Information

ABSTRACT: Unspecific peroxygenases (UPOs) are fungal secreted counterparts of the cytochrome P450 monooxygenases present in most living cells. Both enzyme types share the ability to perform selective oxygenation reactions. Moreover, the *Marasmius rotula* UPO (*Mro*UPO) catalyzes reactions of interest compared with the previously described UPOs, including formation of reactive epoxy fatty acids. To investigate substrate epoxidation, the most frequent positions of oleic acid at the *Mro*UPO heme channel were predicted using binding and molecular dynamics simulations. Then, mutations in neighbor residues were designed aiming at modulating the enzyme epoxidation vs hydroxylation ratio. Both the native (wild-type recombinant) *Mro*UPO and the mutated variants were expressed in *Escherichia coli* as active enzymes, and their action on oleic and other fatty acids was investigated by gas chromatography−mass spectrometry in combination with kinetic analyses. Interestingly, a small modification of the channel shape in the I153T variant increased the ratio between epoxidized oleic acid and its additionally hydroxylated derivatives. A fully opposite effect was attained with the double I153F/S156F variant that completely abolished the ability of the *Mro*UPO to epoxidize oleic acid (while no activity was detected for the I153V variant). The rationale for these results was revealed by the substrate positioning in the above computational simulations, which predict a shorter distance between the oleic acid double bond and the oxygen atom of the peroxide-activated heme (compound I) in the I153T variant than in the native enzyme, promoting epoxidation. In contrast, the I153F/S156F double mutation fully prevents the approach of oleic acid in the bent conformation required for double-bond epoxidation, although its (sub)terminal hydroxylation was predicted and experimentally confirmed. The I153T mutation also increased the UPO selectivity on polyunsaturated fatty acid epoxidation, strongly reducing the ratio between simple epoxides and their hydroxylated derivatives, with respect to the native UPO.

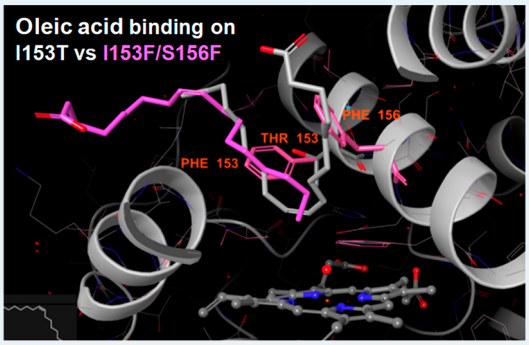

KEYWORDS: *unspecific peroxygenase, Marasmius rotula, unsaturated fatty acids, epoxidation, hydroxylation, computational simulations, PELE software, gas chromatography−mass spectrometry*

INTRODUCTION

The so-called unspecific peroxygenases (UPOs, EC 1.11.2.1) are heme−thiolate enzymes secreted by fungi,[1] whose promiscuous oxygen transfer activities make them "dream catalysts" for difficult oxyfunctionalization reactions of industrial interest.[2] The cysteine ligand of UPO heme iron and the enzyme reaction chemistry are reminiscent of phylogenetically unrelated cytochrome P450 monooxygenases (P450s). Nevertheless, their extracellular nature and consequent higher stability, together with their self-sufficient monooxygenase activity (only requiring H_2O_2 to be activated), confer biotechnological advantages to UPOs.[1]

The first UPO was isolated by Ullrich et al.[3] from the basidiomycete *Agrocybe aegerita* (*Aae*UPO). Additional UPOs have been isolated from cultures of the basidiomycetes *Coprinellus radians* (*Cra*UPO),[4] *Marasmius rotula* (*Mro*UPO),[5] and *Marasmius wettsteinii* (*Mwe*UPO)[6] and the ascomycete *Chaetomium globosum* (*Cgl*UPO).[7] The classical chloroperoxidase from *Leptoxyphium fumago*[8] also belongs to the same protein family, although it exhibits low oxygenation and high halogenation activities compared with UPOs.[1]

Despite the limited number of isolated and characterized members, UPOs are widespread in fungi (and some funguslike organisms) with over 2000 *upo*-type genes identified in sequenced genomes and databases.[1,9] This constitutes a huge repertoire of potential biocatalysts with different oxygen

Received: April 9, 2019
Revised: May 30, 2019

DOI: 10.1021/acscatal.9b01454
ACS Catal. 2019, 9, 6234−6242

transfer capabilities. However, until now only two *upo* genes from genomes/databases (corresponding to the basidiomycete *Coprinopsis cinerea* and the ascomycete *Humicola insolens*) have been heterologously expressed (by Novozymes A/S in *Aspergillus oryzae* host) and the recombinant enzymes (r*Cci*UPO and r*Hin*UPO) already evaluated for oxygenation reactions.[7,10−12]

Heterologous expression is required not only to explore the variety of UPOs in genomes, but also to understand the reaction mechanisms of these enzymes and to tailor their catalytic and operational properties for industrial biocatalysis. Apart from the work of Novozymes mentioned above, additional expression of wild-type *upo* genes as recombinant proteins has not been reported to date. A way to partially solve this limitation came from application of enzyme directed molecular evolution[13] to obtain mutated variants (such as r*Aae*UPO) tailored for expression in *Saccharomyces cerevisiae*,[14] which were later transferred to *Pichia pastoris*.[15] However, the evolved r*Aae*UPO obtained structurally differs from the wild-type enzyme, as shown by comparison of their crystal structures.[16]

As indicated by their systematic name, "substrate:hydrogen-peroxide oxidoreductases (RH-hydroxylating or -epoxidizing)",[17] hydroxylation and epoxidation are the main reactions catalyzed by UPOs. Widespread hydroxylation results in the introduction of alcohol, aldehyde/ketone, and carboxylic acid functionalities by subsequent hydroxylations and dehydration of the resulting *gem*-di/triols as shown for both aromatic[18] and aliphatic[19] compounds. The latter reactions include enzymatic activation of alkanes[20] and production of hydroxylated derivatives of industrial interest.[21]

On the other hand, both olefinic and aromatic compounds are epoxidized by UPOs to different extents. The latter epoxidized compounds easily rearomatize with introduction of a phenolic hydroxyl group.[22,23] However, different alkenes form stable epoxides with *Aae*UPO,[24] in an "activation" reaction of industrial interest.[25] Moreover, epoxidation of unsaturated fatty acids—a main constituent of soybean, linseed, and other plant oils—has high interest for the industrial production of a variety of chemicals and intermediates, including adhesive and binder components among others.[26] Industrial epoxidation of fatty acids is nowadays carried out by the Prileschajew[27] reaction via percarboxylic acids, generated using strong mineral acids as catalysts. To solve the drawbacks of this procedure, the use of the enzyme lipase generating peracids in the presence of H_2O_2 has been proposed.[28] However, this chemoenzymatic approach maintains the drawbacks related to peracid-based epoxidation.

Direct enzymatic epoxidation is catalyzed by P450s[29] and plant peroxygenases.[30] Nevertheless, problems associated with their low stability and frequent requirement for auxiliary substrates and/or enzymes prevent industrial implementation, in spite of numerous studies on their reaction mechanisms.[31−34] Therefore, the recently reported ability of some fungal UPOs to epoxidize unsaturated lipids could be the alternative of choice in the production of industrial epoxides. However, while many substrate oxygenation reactions are shared by different UPOs, fatty acid epoxidation is a characteristic of *Mro*UPO and *Cgl*UPO, while *Aae*UPO and *rCci*UPO do not epoxidize oleic and other unsaturated fatty acids.[35]

To understand and further improve the epoxidation activity of these enzymes, we heterologously expressed a wild-type (i.e., nonmutated) UPO for the first time, obtaining recombinant *Mro*UPO (r*Mro*UPO) as an active enzyme in *Escherichia coli*.[36] Then, guided by computational simulations of substrate diffusion and binding at the crystal-structure active site, we were able to engineer r*Mro*UPO to tune its epoxidizing vs hydroxylating activities on mono- and polyunsaturated (18-carbon) fatty acids.

■ MATERIALS AND METHODS

Computational Simulations. One of the solved crystal structures of *Mro*UPO (PDB 5FUJ, chain A) was used for molecular simulations. The system was optimized at pH 5.5 (*Mro*UPO optimal activity) with the protein preparation wizard from Schrödinger, resulting in histidines 81, 86, 102, and 131 being positively charged (doubly protonated), and the remaining being singly protonated at the δ position. The heme was prepared as the two-electron-oxidized compound I (C-I), a Fe^{4+}═O and porphyrin cation radical complex (see Supporting Information for the force field parameters for heme C-I). Heme charges in all modeling were obtained from a quantum mechanics/molecular mechanics (QM/MM) minimization using QSite,[37] at the DFT M06-L(lacvp*)/OPLS level of theory. In silico mutations were introduced using the side chain prediction routines in Prime.[38]

Three different simulation levels were used to describe the bound protein−ligand complexes. The simplest one involved substrate docking with Glide,[39] using default settings and the single precision SP option. Then, the new adaptive-PELE (Protein Energy Landscape Exploration) software[40] was applied to study substrate diffusion and local conformational sampling. The new protocol improves sampling by running multiple short simulations (epochs) where the initial conditions in each of them are selected through a reward function aiming at sampling nonvisited areas. PELE simulation involved 96 computing cores (trajectories) with 20 epochs of 12 PELE steps each. Interaction energies, in kilocalories per mole, were derived as $E_{ab} - (E_a + E_b)$, where E_{ab} is the total energy of the complex, E_a is the energy of the enzyme, and E_b is the energy of the substrate; all of them were obtained at the OPLS2005 level of theory with a surface GB implicit solvent model. Finally, molecular dynamics (MD) simulations were obtained with Desmond.[41] Initial structures (from Glide) were solvated and equilibrated with the default settings in Desmond. A 250 ns production trajectory was then produced with a Nosé−Hoover chain thermostat, relaxation time of 1.0 ps, and a Martyna−Tobias−Klein barostat with isotropic coupling and a relaxation time of 2.0 ps. The RESPA integrator was employed with bonded, near, and far time steps of 2.0, 2.0, and 6.0 fs, respectively. A 9 Å cutoff was used for nonbonded interactions together with the smooth particle mesh Ewald method.

Native Enzyme and Mutated Variants. Wild-type recombinant (hereinafter native) r*Mro*UPO and its I153S, I153T, I153V, and I153F/S156F mutated variants described below were expressed as soluble recombinant proteins in *E. coli* according to the method for native enzyme production, described in the patent under application number EP 18382514.[36] In short, the *mro*upo gene (with no introns) was cloned into the pET23a plasmid under the control of the T7*lac* promoter and transformed into *E. coli* BL21 cells. Bacteria were grown in ZYM-5052 media at 16 °C during 4 days. Then, cells were lysed by addition of lysozyme and sonication, and debris was removed from the soluble fraction

DOI: 10.1021/acscatal.9b01454
ACS Catal. 2019, 9, 6234−6242

by thorough ultracentrifugation. Three chromatographic steps—two anionic at pH 7.0 and one final cationic at pH 4.0—were used to obtain pure enzymes. The last purification step yielded electrophoretically homogeneous enzyme (as illustrated for r*Mro*UPO in Figure S1). Enzymes from the second chromatographic step were used when fully purified proteins were not required.

Proper folding and binding of the cofactor to the recombinant enzymes were assessed by inspection of the UV−visible spectrum of their resting state (Figure S2). Spectra were recorded using a Cary 60 spectrophotometer in 10 mM phosphate, pH 7.0. Formation of an adduct between the chemically reduced enzyme (ferrous form) and CO, typical of active heme−thiolate enzymes, was assessed in 250 mM phosphate, pH 8.0 (after addition of $Na_2S_2O_4$ and CO flushing) and used to estimate the enzyme concentration in fully and partially purified samples (Figure S3).[42]

The r*Mro*UPO variants were prepared using the Expand Long Template PCR kit from Roche (Basel, Switzerland) for site-directed mutagenesis. PCR reactions were run using the following DNA oligos harboring the desired mismatches (underlined nucleotides in bold triplets): (i) I153S mutation, 5′-CCGATTTAACTGCGACT**TCC**CCGCTCTTCA-GAATCTG-3′; (ii) I153T mutation, 5′-CCGATT-TAACTGCGACT**ACC**CGCTCTTCAGAATCTG-3′; (iii) I153V mutation, 5′-CCGATTTAACTGC-GACT**GTC**CGCTCTTCAGAATCTG-3′; and (iv) I153F/S156F mutation, 5′-CCGATTTAACTGC-GACT**TTC**CGCTCT**TTC**GAATCTGCG-3′, along with their reverse complementary counterparts.

The PCR reactions (50 μL volume) were carried out in an Eppendorf (Hamburg, Germany) Mastercycler pro-S using 30 ng of template DNA, 500 μM each dNTP, 125 ng of direct and reverse primers, 5 units of Expand Long Template PCR System polymerase mix (Roche), and the manufacturer buffer. Reaction conditions included (i) initial denaturation step of 1 min at 95 °C; (ii) 22 cycles of 30 s at 95 °C, 30 s at 60 °C, and 7 min at 68 °C, each; and (iii) final elongation step of 7 min at 68 °C. The mutated *upo* genes were expressed in *E. coli* as described above.

Chemicals. The following unsaturated fatty acids (*cis* isomers) were obtained from Sigma-Aldrich: oleic (*cis*-9-octadecenoic) acid, linoleic (*cis,cis*-9,12-octadecadienoic) acid, and α-linolenic (*cis,cis,cis*-9,12,15-octadecatrienoic) acid. The following epoxide standards were used: (±)-*cis*-9,10-epoxyoctadecanoic acid and (±)-9(10)-EpOME (9,10-*cis*-epoxidized linoleic acid) from Santa Cruz Biotechnology, (±)-12(13)-EpOME (12,13-*cis*-epoxidized linoleic acid) from Cayman, and (±)-9,10−12,13-diepoxyoctadecanoic acid from Larodan.

As standards of epoxidized α-linolenic acid were not available, they were chemically synthesized. With this purpose, a solution of peracetic acid (1.8 mmol) and NaOAc (0.7 mmol) was added to α-linolenic acid (0.5 mmol) using a syringe pump for 1 h at 0 °C. The mixture was stirred for an additional hour at 0 °C and the products were recovered by liquid−liquid extraction with methyl *tert*-butyl ether resulting in a mixture of mono- and diepoxides.

Enzymatic Reactions. Reactions of the above fatty acids (0.1 mM) with r*Mro*UPO and its mutated variants (50−600 nM) were performed in 50 mM sodium phosphate (pH 5.5) at 30 °C and 30−60 min reaction time, in the presence of 1.25−5 mM H_2O_2. Prior to use, the substrates were dissolved in acetone and added to a final acetone concentration of 20% (v/v), although 40% was also tested with some compounds. In control experiments, substrates were treated under the same conditions but without enzyme. Products were recovered by liquid−liquid extraction with methyl *tert*-butyl ether, and dried under N_2. *N,O*-Bis(trimethylsilyl)trifluoroacetamide (Supelco) was used to prepare trimethylsilyl derivatives that were analyzed by gas chromatography−mass spectrometry (GC−MS) as described below.

Enzyme Kinetics. To study the kinetics of oleic acid oxidation, 1 mL reactions with 100 nM r*Mro*UPO and its mutated variants were carried out. Substrate concentration was varied between 12.5 and 1600 μM, and 20% (v/v) acetone was used as cosolvent. The reactions were initiated with 0.5 mM H_2O_2 and stopped after 3 min by vigorous shaking with 100 μL of 100 mM sodium azide. The time course of the reactions was previously analyzed to ensure that the kinetic parameters are estimated when the reaction rate is still in linear phase. All reactions were carried out in triplicate.

Product quantification was performed by GC−MS, as described below. Means and standard errors for the Michaelis constant (K_m) and turnover number (k_{cat}) values were obtained by nonlinear-least-squares fitting to the Michaelis−Menten model. Fitting of these constants to the normalized equation $v = (k_{cat}/K_m)[S]/(1 + [S]/K_m)$ yielded the catalytic efficiencies (k_{cat}/K_m) with their standard errors.

GC−MS Analyses. Chromatographic analyses were performed with a Shimadzu GC−MS QP2010 Ultra equipment, using a fused-silica DB-5HT capillary column (30 m × 0.25 mm internal diameter, 0.1 μm film thickness) from J&W Scientific. The oven was heated from 120 (1 min) to 300 °C (15 min) at 5 °C·min^{-1}. The injection was performed at 300 °C, and the transfer line was kept at 300 °C. Compounds were identified using authentic standards, by mass fragmentography, and comparing their mass spectra with those of the Wiley and NIST libraries. Quantifications were obtained from total-ion peak areas, using external standard curves and molar response factors of the same or similar compounds.

RESULTS AND DISCUSSION

***Mro*UPO Structure.** Although a publication on the crystal structure of *Mro*UPO has not been produced, two sets of atomic coordinates are available at the Protein Data Bank (PDB), as entries 5FUJ and 5FUK (Figure S4 illustrates the dimeric nature of the enzyme, and shows one of the heme access channels). Moreover, some structural features of this enzyme have already been discussed together with their use in oxyfunctionalization reactions.[6,43,44] Among them, the active-site access channel (Figure 1A), and the heme environment residues (Figure 1B) Glu157 and His86 helping the enzyme reaction with H_2O_2, Cys17 acting as the fifth ligand of the heme iron,[1] and the channel residues are relevant to explain the catalytic activities of *Mro*UPO on different substrates, including fatty acids.

Binding of Oleic Acid in *Mro*UPO. Binding of oleic acid in the computationally simulated C-I of *Mro*UPO, using the Glide and PELE softwares, showed analogous results: the unsaturated fatty acid accesses the heme channel in a fully bent conformation (Figures 2A and 3A). This contrasts with the binding of saturated stearic acid, analyzed for comparison, which adopted an extended conformation with ω-1 being the closest position to the oxygen atom of the C-I oxo group (Figure 2B).

DOI: 10.1021/acscatal.9b01454
ACS Catal. 2019, 9, 6234−6242

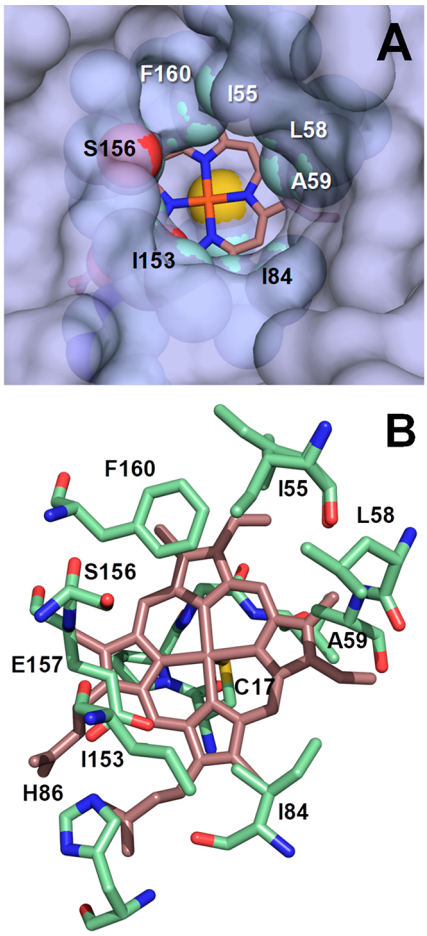

Figure 1. Axial view of the heme channel and environment in *Mro*UPO. (A) Semitransparent solvent access surface with residues forming the channel edge as van der Waals spheres and the heme cofactor as sticks. (B) Disposition of the heme cofactor and surrounding residues from the same orientation shown in (A). Residues are shown with CPK-colored atoms, while the heme cofactor is CPK-colored in (A) and pink in B (Cys17 sulfur is also visible as a yellow sphere in (A)). From PDB 5FUJ.

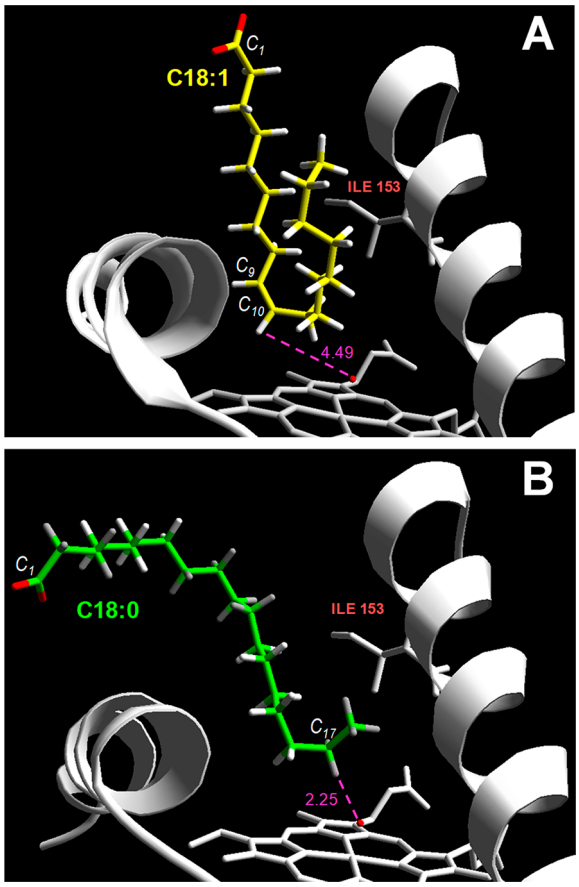

Figure 2. Initial Glide docking of oleic (*cis*-9-octadecenoic, A) and stearic (octadecanoic, B) acids (C18:1 and C18:0 as CPK-colored sticks with yellow and green carbons, respectively) on *Mro*UPO (detail of ribbon model) with indication of distances (in Å) between the C-I oxygen atom (red sphere) and the substrate C_{10} (A) and C_{17} (B) hydrogens. Ile153 to be mutated (see Figure 4) and heme cofactor are shown as white sticks.

A more detailed analysis of the oleic acid position inside the channel (i) identified Ile153 as a residue potentially limiting the approach of the substrate $C_9{=}C_{10}$ double bond to the C-I oxygen atom to be transferred (Figure 2A), (ii) suggested that substitution of Ile153 by a slightly less voluminous residue (as illustrated in Figure 4A for the in silico-mutated I153T variant) could result in shorter Fe═O···HC_{10} distance (Figure S5) and improved epoxidation, and (iii) on the contrary, predicted that the double I153F/S156F mutation could abolish the epoxidation activity by preventing the approach of oleic acid in the required bent conformation (Figures 3 and 4). This is because, due to the introduction of two phenylalanines, the latter in silico variant has a narrower heme channel than the native *Mro*UPO and I153T variant (Figure S6).

Oleic Acid Reactions with r*Mro*UPO Variants. Simple (I153S, I153T, and I153V) and double (I153F/S156F) mutations—which could potentially improve or abolish, respectively, the epoxidation ability of *Mro*UPO (see above)—were experimentally introduced by site-directed mutagenesis. The mutated genes were transformed into *E. coli*, and the same protocol used for the native enzyme[36] was applied to produce the mutated variants. However, only I153T, I153V, and I153F/S156F could be obtained as soluble active enzymes and subsequently purified, with I153V lacking activity on oleic acid and other fatty acids. Interestingly, in *Aae*UPO and *Cci*UPO a threonine residue already occupies the position homologous to *Mro*UPO Ile153.[43] This agrees with the successful production of the I153T variant as an active enzyme, compared with the negative results obtained when a serine or a valine residue was introduced.

The I153T, I153F/S156F, and I153V variants were purified to homogeneity, maintaining the spectroscopic properties of native r*Mro*UPO (Figure S2). Then, their epoxidizing and hydroxylating abilities on oleic (Figure 5) and other unsaturated fatty acids were evaluated by GC−MS, as previously described for the wild *Mro*UPO isolated from fungal cultures.[35]

The most dramatic effect on enzyme activity corresponded to the I153F/S156F variant, whose reaction products (Figure 5C) were restricted to (ω-1) and ω hydroxy, keto, and carboxy derivatives of oleic acid (compared with the native enzyme epoxidized products shown in Figure 5A). The rationale for this result is illustrated by the PELE plots of substrate diffusion shown in Figure 6. The red spots show that the oleic acid C_{18} (ω position) easily attains catalytically relevant distances (at <4 Å from the C-I oxo group) with good interaction energies. Similar distances/energies are found for the more reactive C_{17}

DOI: 10.1021/acscatal.9b01454
ACS Catal. 2019, 9, 6234−6242

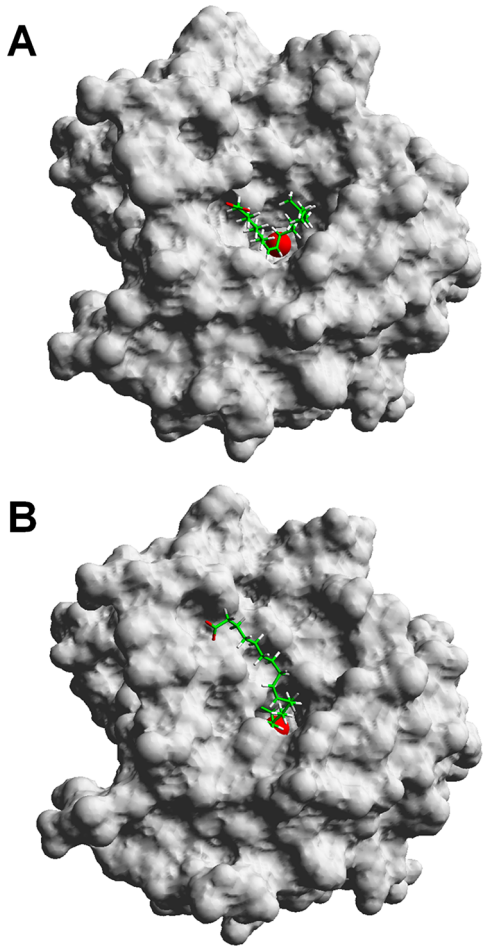

Figure 3. Solvent accessible surfaces of the I153T (A) and I153F/S156F (B) in silico variants of *Mro*UPO (monomer) showing, respectively, the bent and extended binding of oleic acid (CPK-colored sticks) at the heme access channel, as predicted by Glide, with the C-I oxygen atom at the bottom of the channel (as a red van der Waals sphere).

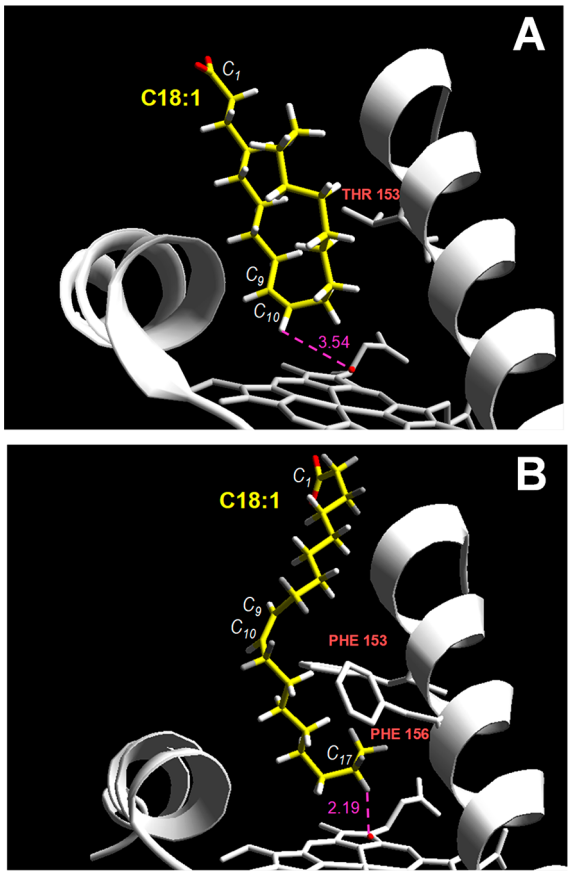

Figure 4. Initial Glide docking of oleic acid (18:1 as CPK-colored sticks) on the I153T (A) and I153F/S156F (B) in silico variants of *Mro*UPO (detail of ribbon model) with indication of distances (in Å) between the C-I oxygen atom (red sphere) and the substrate C_{10} (A) and C_{18} (B) hydrogens. Mutated residues (Thr153 in (A) and Phe153 and Phe156 in (B)) and heme cofactor are shown as white sticks.

(ω-1) position. This should favor (sub)terminal hydroxylation, in agreement with the experimental results. In contrast, the C_{10} (blue spots) atom always remains too far (>5 Å) and good interaction energies are only observed at long distances (>10 Å) from the C-I oxo group, preventing epoxidation of the double bond.

However, the most interesting effect observed is the improvement in the already described fatty acid epoxidation activity of *Mro*UPO,[35] as a result of the I153T mutation (Figure 5, parts A and B, respectively). Oleic acid epoxidation is observed in both cases, but its selectivity increased in the I153T reaction with significantly lower amounts of (ω-7)- and (ω-1)-hydroxylated epoxidized derivatives (Figure 5B) under the present conditions (the chemical structures of oleic acid products are shown in Figure S7, left). Due to the slight difference between the variants, for modeling justification we made use of (more precise) MD simulations this time.

The active site dynamics of oleic acid in *Mro*UPO and its I153T variant (Figure 7, parts A and B, respectively) show a significantly shorter average distance from the oleic acid double bond (between C_9 and C_{10}) to the C-I reactive oxygen in I153T, compared with the native enzyme. This agrees with the shortened distance (3.5 vs 4.5 Å) already observed in the initial docking (Figures 4A and 2A, respectively).

The modeling by PELE, addressing the ligand entrance into the active site (Figure S8), strongly supports the MD local sampling. The I153T variant presents a minimum at distances (oxo−C_{10}) of ∼3 Å, whereas *Mro*UPO presents the minima at distances of ∼6 Å, with a significant total energy increase at lower distances.

Reaction on Polyunsaturated Fatty Acids. Epoxidation of polyunsaturated fatty acids presents additional industrial interest since the introduction of several epoxy functionalities in the same molecule results in higher cross-linking potential. Therefore, linoleic and α-linolenic fatty acids were also evaluated as substrates of the enzyme (Figure 8).

Diepoxides (*syn* and *anti* isomers) and hydroxylated mono- and diepoxides are the main products of the r*Mro*UPO and its I153T variant reactions with linoleic acid (Figure 8, parts A and B, respectively). As in the oleic acid reactions, the amount of hydroxylated epoxides was lower with the I153T variant (the chemical structures of linoleic acid products are shown in Figure S7, center).

More interestingly, while a variety of other (additionally oxygenated) α-linolenic acid epoxidized derivatives were observed in the native r*Mro*UPO reactions (Figure 8C), nearly selective synthesis of diepoxides was obtained in the I153T

DOI: 10.1021/acscatal.9b01454
ACS Catal. 2019, 9, 6234−6242

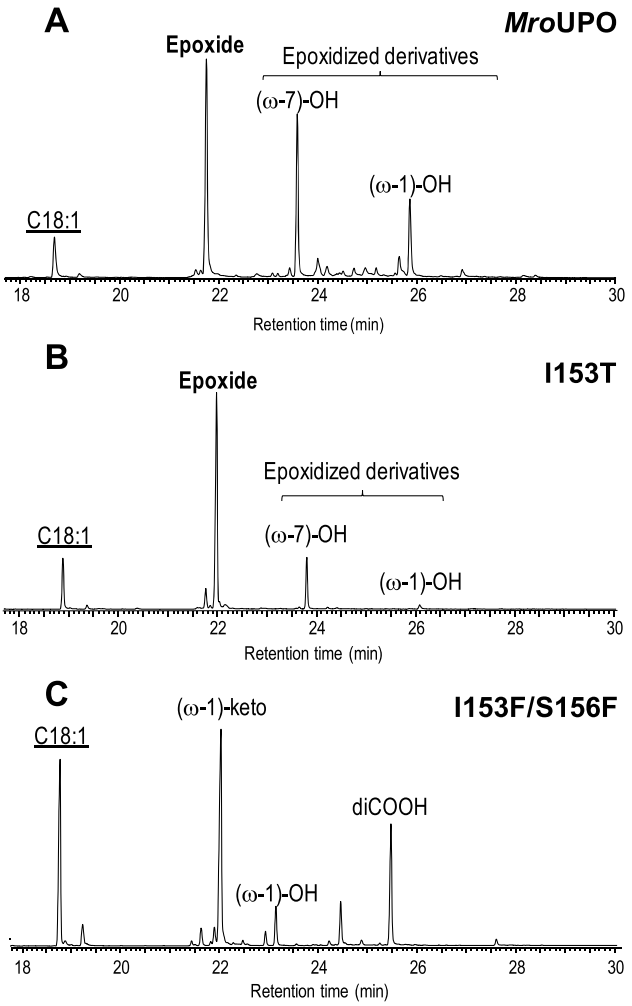

Figure 5. GC–MS analysis of oleic acid (C18:1, underlined) reactions with native r*Mro*UPO (A) and its I153T (B) and I153F/S156F (C) variants. Simple epoxides (bold) and additionally oxygenated epoxidized derivatives are the main products in (A) and (B), while only products from subterminal and terminal oxygenation are shown in (C). The reactions were performed with 100 μM substrate, 0.2 μM enzyme and 2.5 mM H_2O_2 for 30 min.

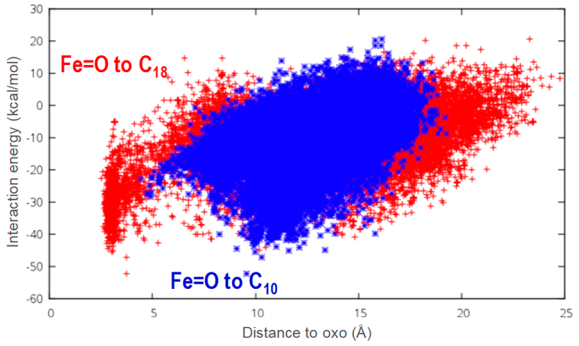

Figure 6. PELE diffusion of oleic acid on the I153F/S156F in silico variant of *Mro*UPO. The distances from substrate C_{10} (blue spots) and C_{18} (red spots) to the C-I oxo group are shown on the *x*-axis, and the corresponding interaction energies are shown on the *y*-axis.

reactions (Figure 8D) (the chemical structures of α-linolenic acid products are shown in Figure S7, right).

Kinetic Constants and Products. Despite difficulties in obtaining maximal (initial) reaction rates from chromatographic analyses of enzymatic reactions, the kinetics of oleic acid oxyfunctionalization by r*Mro*UPO and its two mutated variants could be analyzed in the range of 5–1600 μM substrate concentration (Figure 9).

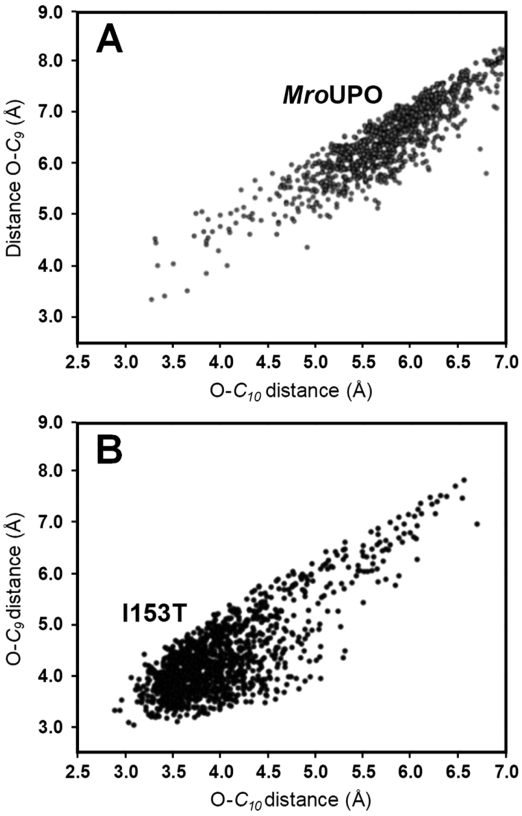

Figure 7. Positions of oleic acid after MD at the heme channel of *Mro*UPO (A) and its I153T variant (B) as shown by distances between the C-I oxo group and the C_{10} (*x*-axis) and C_9 (*y*-axis) atoms of the substrate.

The kinetic constants obtained (Table 1) revealed that the I153T mutation increases UPO catalytic efficiency (k_{cat}/K_m) epoxidizing oleic acid due to a significant improvement of the k_{cat} (from 1.5 ± 0.1 to 2.1 ± 0.1 s^{-1}). This is in agreement with computational simulations showing a shorter distance between the substrate double bond and the C-I oxo group (Figure 7), which will favor the electron and oxygen transfers. The experimental results also confirm the loss of epoxidizing ability and the new ω-1/ω hydroxylating ability of the I153F/S156F variant, predicted by PELE. Interestingly, the (sub)terminal hydroxylation activity by this variant (k_{cat} 2.3 ± 0.1 s^{-1}) is similar to the total oxygenation activity of the native r*Mro*UPO (k_{cat} 2.0 ± 0.2 s^{-1}) although lower than that of the I153T variant (k_{cat} 3.6 ± 0.1 s^{-1}) (Figure 9 and Table 1).

The time course of the epoxidation and additional oxygenation reactions (as shown in Figure S9 for the I153T variant) showed that the (ω-7)-hydroxylated and epoxidized derivatives of oleic acid are already present at the shorter reaction time (1 min), while doubly oxygenated (hydroxylated plus epoxidized) oleic acid appears later. Interestingly, reactions with a standard of epoxidized oleic (9,10-epoxystearic) acid failed to show hydroxylation at the allylic (C_{11}) position (data not shown), suggesting that (ω-7)-hydroxyoleic acid is the precursor of the doubly oxygenated derivative in the r*Mro*UPO reactions.

DOI: 10.1021/acscatal.9b01454
ACS Catal. 2019, 9, 6234–6242

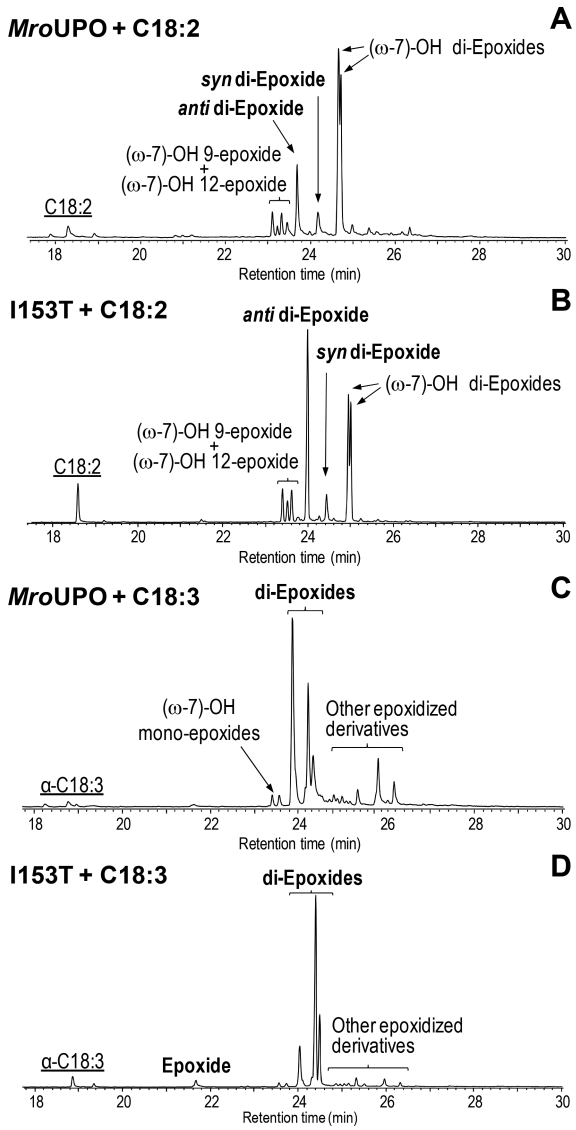

Figure 8. GC−MS analysis of reactions of linoleic (C18:2) and α-linolenic (C18:3) acids (substrates underlined) with native *Mro*UPO (A and C, respectively) and its I153T variant (B and D, respectively). Simple diepoxides (*anti* and *syn* isomers from linoleic acid in (A) and (B), and three unassigned isomers from α-linolenic in (C) and (D), bold) and other epoxidized derivatives are the main reaction products. The reactions were performed with 100 μM substrate, 0.6 (A and B) or 0.2 μM (C and D) enzyme, and 1.25 mM H_2O_2 for 30−60 min.

For quantitative comparison of the epoxidized products obtained, r*Mro*UPO and I153T reactions were performed under conditions (enzyme dose and/or reaction time) resulting in nearly complete (85−98%) conversion of the unsaturated fatty acids (Table 2). Then, the percentages of "only epoxidized" (mono- and diepoxides) and total epoxidized derivatives (including hydroxy- and oxoepoxides) were calculated. In these reactions, the I153T mutation increased *Mro*UPO selectivity epoxidizing the three fatty acids assayed, with the highest improvement (15-fold) with respect to native r*Mro*UPO being obtained for α-linolenic acid. In this way, up to 85% conversion of α-linolenic acid into diepoxy-octadecenoic acid was attained using the I153T variant of r*Mro*UPO.

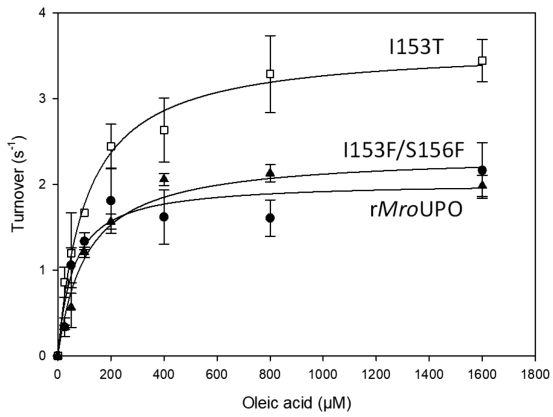

Figure 9. Comparison of kinetics of oleic acid reactions (total oxygenated products in Figure 5) with r*Mro*UPO (circles) and its I153T (squares) and I153F/S156F (triangles) variants.

Table 1. Kinetic Constants of r*Mro*UPO and Its I153T and I153F/S156F Variants in Oleic Acid Reactions Considering (i) All Epoxidized Products, (ii) Products Only Hydroxylated, and (ii) Total Oxygenated Products[a,b]

	k_{cat} (s^{-1})	K_m (μM)	k_{cat}/K_m ($s^{-1}\cdot mM^{-1}$)
(i) all epoxidized products			
r*Mro*UPO	1.5 ± 0.1	52 ± 15	29 ± 8
I153T	2.1 ± 0.1	58 ± 8	36 ± 5
I153F/S156F	0	–	0
(ii) products only hydroxylated			
r*Mro*UPO	0.6 ± 0.0	61 ± 20	10 ± 3
I153T	1.4 ± 0.1	122 ± 17	11 ± 2
I153F/S156F	2.3 ± 0.1	108 ± 24	21 ± 5
(iii) total oxygenated products			
r*Mro*UPO	2.0 ± 0.2	64 ± 21	31 ± 11
I153T	3.6 ± 0.1	100 ± 13	36 ± 5
I153F/S156F	2.3 ± 0.1	108 ± 24	21 ± 5

[a]Note that only hydroxylation is produced by the I153F/S156F variant. [b]Means and 95% standard deviations.

Table 2. Molar Conversion, Percentages of Fatty Acid Derivatives (i) with Only Epoxides and (ii) Bearing Epoxides plus Other New Oxygenated Functions, and Epoxidation Selectivity, after Nearly Complete Conversion of Oleic (18:1), Linoleic (18:2), and α-Linolenic (18:3) Acids by r*Mro*UPO and Its I153T Variant (as Percentages of Total Chromatographied Products)[a]

		conversion	(i) only epoxides	(ii) other epoxides	selectivity[b]
18:1	r*Mro*UPO	94	40	57	0.67
	I153T	85	72	17	2.67
18:2	r*Mro*UPO	98	21	79	0.27
	I153T	93	42	58	0.72
18:3	r*Mro*UPO	98	44	56	0.79
	I153T	97	92 (4/88)	8	11.50

[a]Monoepoxide/diepoxide derivatives of α-linolenic acid are indicated in parentheses. [b]Epoxidation selectivity = ratio between only epoxides and other oxygenation products

DOI: 10.1021/acscatal.9b01454
ACS Catal. 2019, 9, 6234−6242

CONCLUSIONS

Based on computational simulations of oleic acid diffusion on the *Mro*UPO crystal structure, some mutations were designed to modulate the epoxidation vs hydroxylation activities of the enzyme, an important aspect to produce reactive compounds of industrial interest. Then, *E. coli* expression was used for the first time to produce UPO variants (bearing the previously designed mutations) which were obtained in soluble and active form. Finally, GC−MS analyses of unsaturated fatty acid reactions with the purified mutated variants confirmed their new/improved catalytic properties.

Using this combined approach, we show that the *Mro*UPO epoxidation activity on oleic acid can be removed by the double I153F/S156F mutation, which limits substrate entrance in the bent position required to approach its double bond to the reactive oxygen of the heme C-I. More interestingly, we also show that the epoxidation selectivity of the enzyme (on oleic, linoleic, and α-linolenic acids) can be improved by the I153T mutation that reduces the distance between the oleic double bond and the C-I oxygen atom to be transferred to the substrate.

In P450s, the ratio between epoxidation and hydroxylation activities has been associated with differences in the formation of enzyme reactive species (compounds 0 and I with hydroperoxo and oxenoid iron) involving an active-site threonine.[31,33] Strikingly, we report here that introduction of a threonine residue at the r*Mro*UPO active site results in more selective epoxidation. However, the effect of the latter mutation is due to more favorable positioning of the substrate (as shown by computational simulations) instead of an effect on the ratio between r*Mro*UPO reactive species (note that a glutamic acid, Glu157, plays in this UPO the role proposed for conserved threonine in P450s).[1]

In summary, we provide here the first example on UPO rational design (using *E. coli* expression) that hopefully will be followed by further protein engineering studies on other reactions of interest catalyzed by this and other fungal peroxygenases.

ASSOCIATED CONTENT

Supporting Information

The Supporting Information is available free of charge on the ACS Publications website at DOI: 10.1021/acscatal.9b01454.

> Purification of r*Mro*UPO; UV−visible spectra of r*Mro*UPO and its variants ; UV−visible spectrum of r*Mro*UPO complex with CO; general structure of *Mro*UPO; comparison of oleic acid in simulations; heme channel opening after in silico mutations; formulas of substrate epoxidized derivatives; PELE oleic acid migration in *Mro*UPO; initial time course of oleic acid reaction; methods including force field parameters of heme C-I and resulting spin density (PDF)

AUTHOR INFORMATION

Corresponding Authors

*E-mail: ATMartinez@cib.csic.es.
*E-mail: anagu@irnase.csic.es.
*E-mail: victor.guallar@bsc.es.

ORCID

Alejandro González-Benjumea: 0000-0003-2857-9491
Ana Gutiérrez: 0000-0002-8823-9029
Angel T. Martínez: 0000-0002-1584-2863

Present Address

#Technical University of Delft, The Netherlands.

Author Contributions

⊥J.C., A.G.-B., and E.F.-F.: These authors contributed equally to the work.

Notes

The authors declare no competing financial interest.

ACKNOWLEDGMENTS

This work has been funded by the BBI-JU (www.bbi-europe.eu) project SusBind (on "Sustainable biobinders"; H2020-BBI-JTI-2017-792063; https://susbind.eu), together with the CTQ2016-79138-R and BIO2017-86559-R (GENOBIOREF) projects of the Spanish Ministry of Economy, Industry and Competitiveness, cofinanced by FEDER funds. The authors thank Andrés Olmedo (IRNAS, Sevilla) for his useful comments.

REFERENCES

(1) Hofrichter, M.; Kellner, H.; Pecyna, M. J.; Ullrich, R. Fungal Unspecific Peroxygenases: Heme-Thiolate Proteins that Combine Peroxidase and Cytochrome P450 Properties. *Adv. Exp. Med. Biol.* **2015**, *851*, 341−368.

(2) Wang, Y.; Lan, D.; Durrani, R.; Hollmann, F. Peroxygenases en Route to Becoming Dream Catalysts. What Are the Opportunities and Challenges? *Curr. Opin. Chem. Biol.* **2017**, *37*, 1−9.

(3) Ullrich, R.; Nuske, J.; Scheibner, K.; Spantzel, J.; Hofrichter, M. Novel Haloperoxidase from the Agaric Basidiomycete *Agrocybe aegerita* Oxidizes Aryl Alcohols and Aldehydes. *Appl. Environ. Microbiol.* **2004**, *70*, 4575−4581.

(4) Anh, D. H.; Ullrich, R.; Benndorf, D.; Svatos, A.; Muck, A.; Hofrichter, M. The Coprophilous Mushroom *Coprinus radians* Secretes a Haloperoxidase that Catalyzes Aromatic Peroxygenation. *Appl. Environ. Microbiol.* **2007**, *73*, 5477−5485.

(5) Gröbe, G.; Ullrich, M.; Pecyna, M.; Kapturska, D.; Friedrich, S.; Hofrichter, M.; Scheibner, K. High-Yield Production of Aromatic Peroxygenase by the Agaric Fungus *Marasmius rotula*. *AMB Express* **2011**, *1*, 31−42.

(6) Ullrich, R.; Poraj-Kobielska, M.; Scholze, S.; Halbout, C.; Sandvoss, M.; Pecyna, M. J.; Scheibner, K.; Hofrichter, M. Side Chain Removal from Corticosteroids by Unspecific Peroxygenase. *J. Inorg. Biochem.* **2018**, *183*, 84−93.

(7) Kiebist, J.; Schmidtke, K. U.; Zimmermann, J.; Kellner, H.; Jehmlich, N.; Ullrich, R.; Zänder, D.; Hofrichter, M.; Scheibner, K. A Peroxygenase from *Chaetomium globosum* Catalyzes the Selective Oxygenation of Testosterone. *ChemBioChem* **2017**, *18*, 563−569.

(8) Thomas, J. A.; Morris, D. R.; Hager, L. P. Chloroperoxidase. *J. Biol. Chem.* **1970**, *245*, 3135−3142.

(9) Pecyna, M.; Molekularbiologische Charakterisierung von Hämthiolat- und DYP-type-Peroxidasen ausgewählter Basidiomyceten. Ph.D.Thesis, TU-Dresden, 2016.

(10) Babot, E. D.; del Río, J. C.; Kalum, L.; Martínez, A. T.; Gutiérrez, A. Oxyfunctionalization of Aliphatic Compounds by a Recombinant Peroxygenase from *Coprinopsis cinerea*. *Biotechnol. Bioeng.* **2013**, *110*, 2323−2332.

(11) Babot, E. D.; del Río, J. C.; Kalum, L.; Martínez, A. T.; Gutiérrez, A. Regioselective Hydroxylation in the Production of 25-Hydroxyvitamin D by *Coprinopsis cinerea* Peroxygenase. *ChemCatChem* **2015**, *7*, 283−290.

(12) Aranda, C.; Municoy, M.; Guallar, V.; Kiebist, J.; Scheibner, K.; Ullrich, R.; del Río, J. C.; Hofrichter, M.; Martínez, A. T.; Gutiérrez, A. Selective Synthesis of 4-Hydroxyisophorone and 4-Ketoisophorone by Fungal Peroxygenases. *Catal. Sci. Technol.* **2019**, *9*, 1398−1405.

(13) Schmidt-Dannert, C.; Arnold, F. H. Directed Evolution of Industrial Enzymes. *Trends Biotechnol.* **1999**, *17*, 135−136.

DOI: 10.1021/acscatal.9b01454
ACS Catal. 2019, 9, 6234−6242

(14) Molina-Espeja, P.; Garcia-Ruiz, E.; Gonzalez-Perez, D.; Ullrich, R.; Hofrichter, M.; Alcalde, M. Directed Evolution of Unspecific Peroxygenase from *Agrocybe aegerita*. *Appl. Environ. Microbiol.* **2014**, *80*, 3496−3507.
(15) Molina-Espeja, P.; Ma, S.; Maté, D. M.; Ludwig, R.; Alcalde, M. Tandem-Yeast Expression System for Engineering and Producing Unspecific peroxygenase. *Enzyme Microb. Technol.* **2015**, *73*−*74*, 29−33.
(16) Ramírez-Escudero, M.; Molina-Espeja, P.; Gómez de Santos, P.; Hofrichter, M.; Sanz-Aparicio, J.; Alcalde, M. Structural Insights into the Substrate Promiscuity of a Laboratory Evolved Peroxygenase. *ACS Chem. Biol.* **2018**, *13*, 3259−3268.
(17) Moss, G. P. Enzyme Nomenclature. Recommendations of the Nomenclature Committee of the International Union of Biochemistry and Molecular Biology on the Nomenclature and Classification of Enzymes by the Reactions they Catalyse. https://www.qmul.ac.uk/sbcs/iubmb/enzyme (accessed Feb 21, 2019).
(18) Kinne, M.; Zeisig, C.; Ullrich, R.; Kayser, G.; Hammel, K. E.; Hofrichter, M. Stepwise Oxygenations of Toluene and 4-Nitrotoluene by a Fungal Peroxygenase. *Biochem. Biophys. Res. Commun.* **2010**, *397*, 18−21.
(19) Gutiérrez, A.; Babot, E. D.; Ullrich, R.; Hofrichter, M.; Martínez, A. T.; del Río, J. C. Regioselective Oxygenation of Fatty Acids, Fatty Alcohols and Other Aliphatic Compounds by a Basidiomycete Heme-Thiolate Peroxidase. *Arch. Biochem. Biophys.* **2011**, *514*, 33−43.
(20) Olmedo, A.; Aranda, C.; del Río, J. C.; Kiebist, J.; Scheibner, K.; Martínez, A. T.; Gutiérrez, A. From Alkanes to Carboxylic Acids: Terminal Oxygenation by a Fungal Peroxygenase. *Angew. Chem., Int. Ed.* **2016**, *55*, 12248−12251.
(21) Lund, H.; Brask, J.; Kalum, L.; Gutiérrez, A.; Babot, E. D.; Ullrich, R.; Hofrichter, M.; Martínez, A. T.; del Río, J. C. *Enzymatic Preparation of Diols*. World Patent WO2013/004639A2, Int. Patent 12249-EP-EPA, U.S. Patent US20140234917, 2014.
(22) Kluge, M.; Ullrich, R.; Dolge, C.; Scheibner, K.; Hofrichter, M. Hydroxylation of Naphthalene by Aromatic Peroxygenase from *Agrocybe aegerita* Proceeds via Oxygen Transfer from H_2O_2 and Intermediary Epoxidation. *Appl. Microbiol. Biotechnol.* **2009**, *81*, 1071−1076.
(23) Karich, A.; Kluge, M.; Ullrich, R.; Hofrichter, M. Benzene Oxygenation and Oxidation by the Peroxygenase of *Agrocybe aegerita*. *AMB Express* **2013**, *3*, 5.
(24) Peter, S.; Kinne, M.; Ullrich, R.; Kayser, G.; Hofrichter, M. Epoxidation of Linear, Branched and Cyclic Alkenes Catalyzed by Unspecific Peroxygenase. *Enzyme Microb. Technol.* **2013**, *52*, 370−376.
(25) Lund, H.; Kalum, L.; Hofrichter, M.; Peter, S. *Epoxidation Using Peroxygenase*. U.S. Patent US 9908860 B2, 2018.
(26) Corma, A.; Iborra, S.; Velty, A. Chemical Routes for the Transformation of Biomass into Chemicals. *Chem. Rev.* **2007**, *107*, 2411−2502.
(27) Prileschajew, N. Oxydation ungesättigter Verbindungen mittels organischer Superoxyde. *Ber. Dtsch. Chem. Ges.* **1909**, *42*, 4811−4815.
(28) Björkling, F.; Frykman, H.; Godtfredsen, S. E.; Kirk, O. Lipase Catalyzed Synthesis of Peroxycarboxylic Acids and Lipase Mediated Oxidations. *Tetrahedron* **1992**, *48*, 4587−4592.
(29) Ruettinger, R. T.; Fulco, A. J. Epoxidation of Unsaturated Fatty-Acids by a Soluble Cytochrome P-450-Dependent System from *Bacillus megaterium*. *J. Biol. Chem.* **1981**, *256*, 5728−5734.
(30) Piazza, G. J.; Nuñez, A.; Foglia, T. A. Epoxidation of Fatty Acids, Fatty Methyl Esters, and Alkenes by Immobilized Oat Seed Peroxygenase. *J. Mol. Catal. B: Enzym.* **2003**, *21*, 143−151.
(31) Vaz, A. D. N.; McGinnity, D. F.; Coon, M. J. Epoxidation of Olefins by Cytochrome P450: Evidence from Site-Specific Mutagenesis for Hydroperoxo-Iron as an Electrophilic Oxidant. *Proc. Natl. Acad. Sci. U. S. A.* **1998**, *95*, 3555−3560.
(32) Kubo, T.; Peters, M. W.; Meinhold, P.; Arnold, F. H. Enantioselective Epoxidation of Terminal Alkenes to (R)- and (S)-Epoxides by Engineered Cytochromes P450 BM-3. *Chem. - Eur. J.* **2006**, *12*, 1216−1220.
(33) Hrycay, E. G.; Bandiera, S. M. Monooxygenase, Peroxidase and Peroxygenase Properties and Reaction Mechanisms of Cytochrome P450 Enzymes. *Adv. Exp. Med. Biol.* **2015**, *851*, 1−61.
(34) Wang, L.; Wei, S. P.; Pan, X. C.; Liu, P. X.; Du, X.; Zhang, C.; Pu, L.; Wang, Q. Enhanced Turnover for the P450 119 Peroxygenase-Catalyzed Asymmetric Epoxidation of Styrenes by Random Mutagenesis. *Chem. - Eur. J.* **2018**, *24*, 2741−2749.
(35) Aranda, C.; Olmedo, A.; Kiebist, J.; Scheibner, K.; del Río, J. C.; Martínez, A. T.; Gutiérrez, A. Selective Epoxidation of Fatty Acids and Fatty Acid Methyl Esters by Fungal Peroxygenases. *ChemCatChem* **2018**, *10*, 3964−3968.
(36) Fernández-Fueyo, E.; Aranda, C.; Gutiérrez, A.; Martínez, A. T. Eur. Patent EP18382514.0, 2018.
(37) *QSite 4.5*; Schrödinger, LLC.: Portland, OR, 2007.
(38) *Prime*, release 2019-1; Schrödinger, LLC: New York, 2019.
(39) Friesner, R. A.; Banks, J. L.; Murphy, R. B.; Halgren, T. A.; Klicic, J. J.; Mainz, D. T.; Repasky, M. P.; Knoll, E. H.; Shelley, M.; Perry, J. K.; Shaw, D. E.; Francis, P.; Shenkin, P. S. Glide: A New Approach for Rapid, Accurate Docking and Scoring. 1. Method and Assessment of Docking Accuracy. *J. Med. Chem.* **2004**, *47*, 1739−1749.
(40) Lecina, D.; Gilabert, J. F.; Guallar, V. Adaptive Simulations, towards Interactive Protein-Ligand Modeling. *Sci. Rep.* **2017**, *7*, 8466.
(41) Bowers, K. J.; Chow, E.; Xu, H.; Dror, R. O.; Eastwood, M. P.; Gregersen, B. A.; Klepeis, J. L.; Kolossváry, I.; Moraes, M. A.; Sacerdoti, F. D.; Salmon, J. K.; Shan, Y.; Shaw, D. E. Scalable Algorithms for Molecular Dynamics Simulations on Commodity Clusters. *Proceedings of ACM/IEEE Conference on Supercomputing (SC06), Tampa, FL, Nov 11−17, 2006*; IEEE: 2006; p 43..
(42) Otey, C. R. High-Throughput Carbon Monoxide Binding Assay for Cytochromes P450. *Methods Mol. Biol.* **2003**, *230*, 137−139.
(43) Aranda, C.; Ullrich, R.; Kiebist, J.; Scheibner, K.; del Río, J. C.; Hofrichter, M.; Martínez, A. T.; Gutiérrez, A. Selective Synthesis of the Resveratrol Analogue 4,4′-Dihydroxy-*trans*-Stilbene and Stilbenoids Modification by Fungal Peroxygenases. *Catal. Sci. Technol.* **2018**, *8*, 2394−2401.
(44) Olmedo, A.; del Río, J. C.; Kiebist, J.; Scheibner, K.; Martínez, A. T.; Gutiérrez, A.; Ullrich, R.; Hofrichter, M. Fatty Acid Chain Shortening by a Fungal Peroxygenase. *Chem. - Eur. J.* **2017**, *23*, 16985−16989.

DOI: 10.1021/acscatal.9b01454
ACS Catal. 2019, 9, 6234−6242

SUPPORTING INFORMATION

Modulating Fatty-Acid Epoxidation *vs* Hydroxylation in a Fungal Peroxygenase

Juan Carro,[§] Alejandro González-Benjumea,[#] Elena Fernández-Fueyo,[§] Carmen Aranda,[#] Victor Guallar,*[¶†] Ana Gutiérrez,*[#] and Angel T. Martínez*[§]

[§]Centro de Investigaciones Biológicas, CSIC, Ramiro de Maeztu 9, E-28040 Madrid, Spain; [#]Instituto de Recursos Naturales y Agrobiología, CSIC, Reina Mercedes 10, E-41012 Sevilla, Spain; [¶]Barcelona Supercomputing Center, Jordi Girona 29, E-08034 Barcelona, Spain; [†]ICREA, Passeig Lluís Companys 23, E-08010 Barcelona, Spain

*E-mail: ATMartinez@cib.csic.es, anagu@irnase.csic.es, guallarv@bsc.es

Supporting information includes: Purification of r*Mro*UPO (**Figure S1**), UV-visible spectra of r*Mro*UPO and its variants (**Figure S2**); UV-visible spectrum of r*Mro*UPO complex with CO (**Figure S3**), General structure of *Mro*UPO (**Figure S4**); Comparison of oleic acid in simulations (**Figure S5**); Heme channel opening after *in silico* mutations (**Figure S6**); Formulae of substrate epoxidized derivatives (**Figure S7**); Initial PELE oleic acid migration in *Mro*UPO (**Figure S8**); time course of oleic acid reaction (**Figure S9**); and Supporting **Material and Methods** including forcefield parameters of heme C-I and resulting spin density (**Figure S10**).

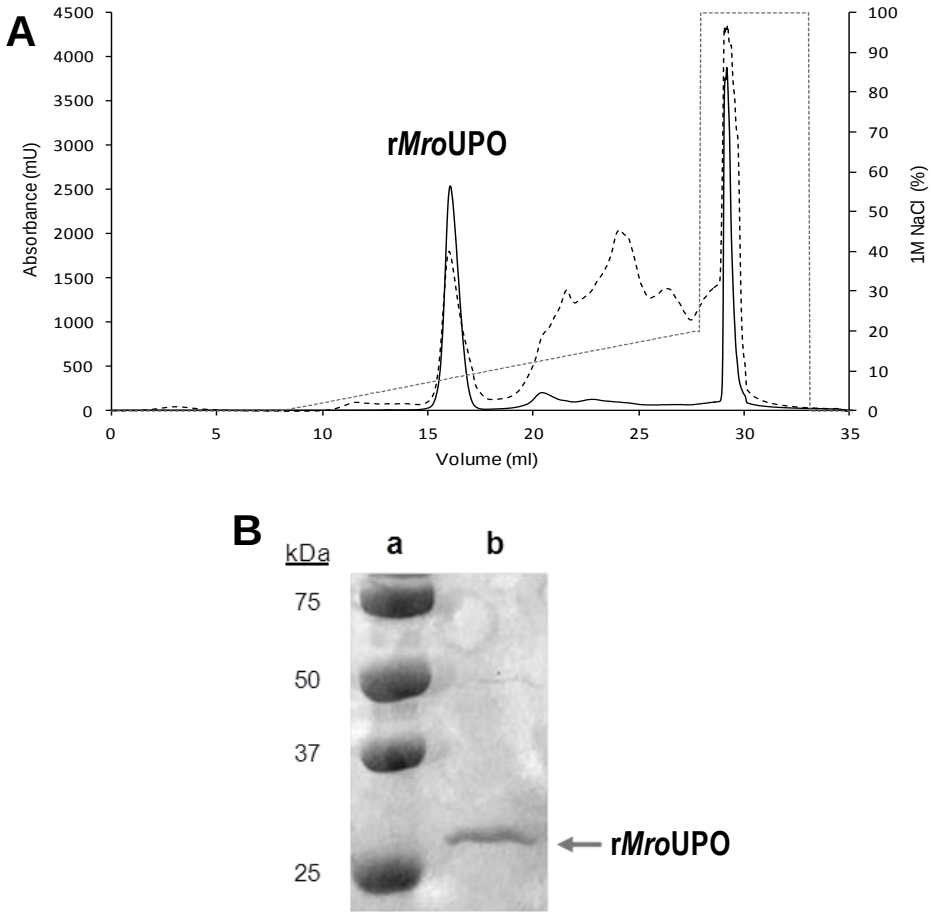

Figure S1. Purification of r*Mro*UPO heterologously expressed in *E. coli* as soluble active enzyme. (**A**) Mono-S chromatography showing 280 nm (dashed line) and 410 nm (continuous line) absorbance profiles and NaCl gradient (dotted line). (**B**) Sodium dodecylsulfate-polyacrylamide gel electrophoresis of purified r*Mro*UPO (*lane b*) compared with molecular-mass standards (*lane a*).

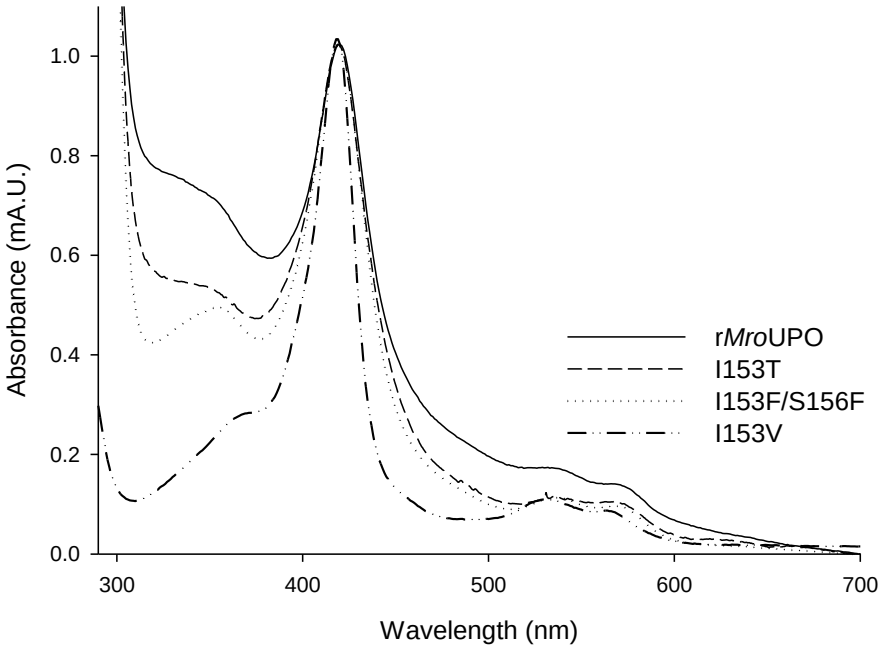

Figure S2. UV-visible spectra of r*Mro*UPO and its I153T, I153F/S156F and I153V variants showing the main Soret band at 420 nm, and two small charge-transfer bands around 530 and 567 nm.

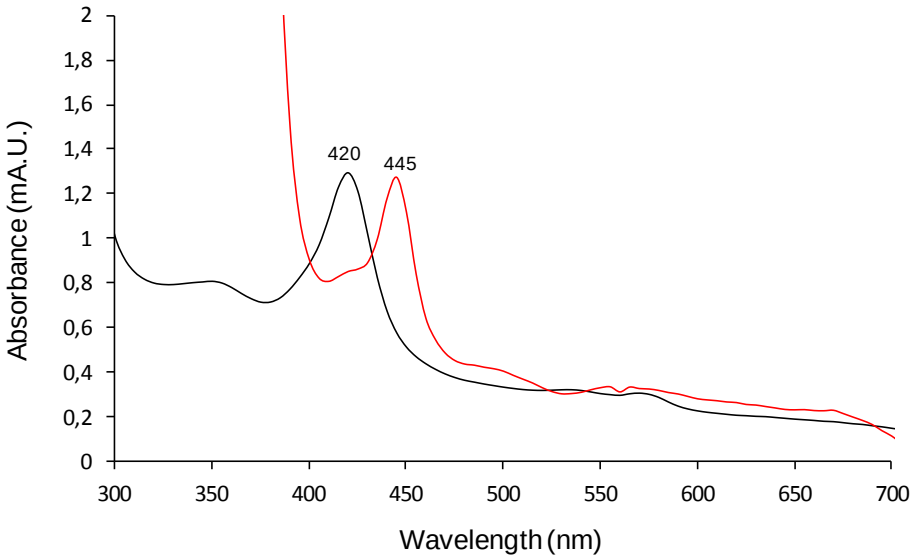

Figure S3. UV-visible spectra of r*Mro*UPO (black line) and its CO complex (red line).

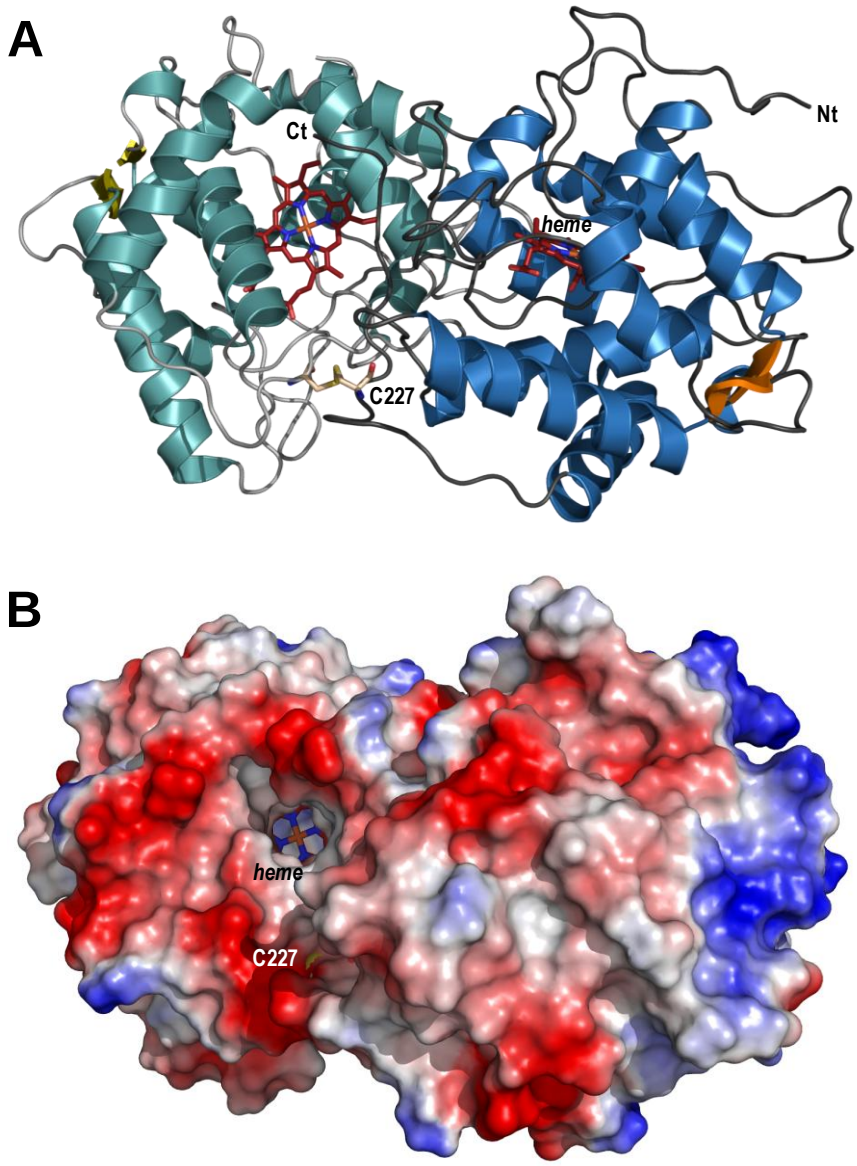

Figure S4. Overall molecular structure of *Mro*UPO dimeric enzyme (PDB 5FUJ). **A**) Ribbon diagram showing the helical secondary structure, N and C termini (Nt and Ct), heme cofactors, and intermolecular (C227-C227) disulfide bridge linking together the two enzyme monomers (heme, Ct, Nt and Cys227 are only labeled on the right monomer; heme and Cys227 residues are shown as CPK-colored sticks). **B)** Solvent access surface showing one of the access channels to heme (CPK-colored sticks) and one of the Cys227 residues (CPK-colored spheres), colored by electrostatic charge (*red*, negative; and *blue* positive).

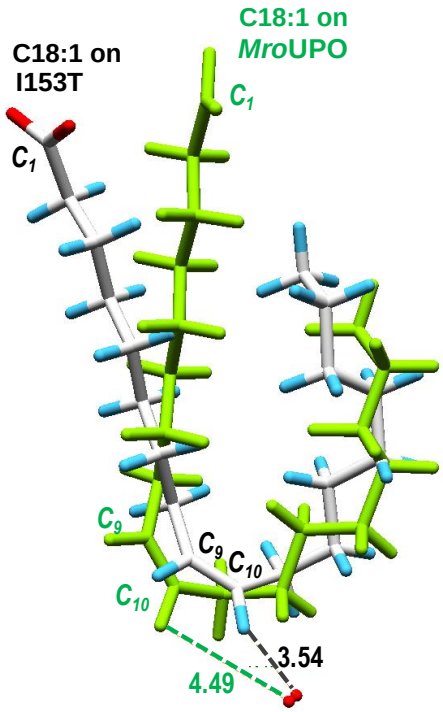

Figure S5. Comparison of oleic acid in *Mro*UPO (green sticks) and its I153T *in silico* variant (CPK sticks) after Glide docking (see **Figures 2B** and **3A**). The distances between the C-I oxygen (red sphere) and the H atom in substrate C_{10} (the double-bond carbon atom closest to heme oxo) are indicated (in Å).

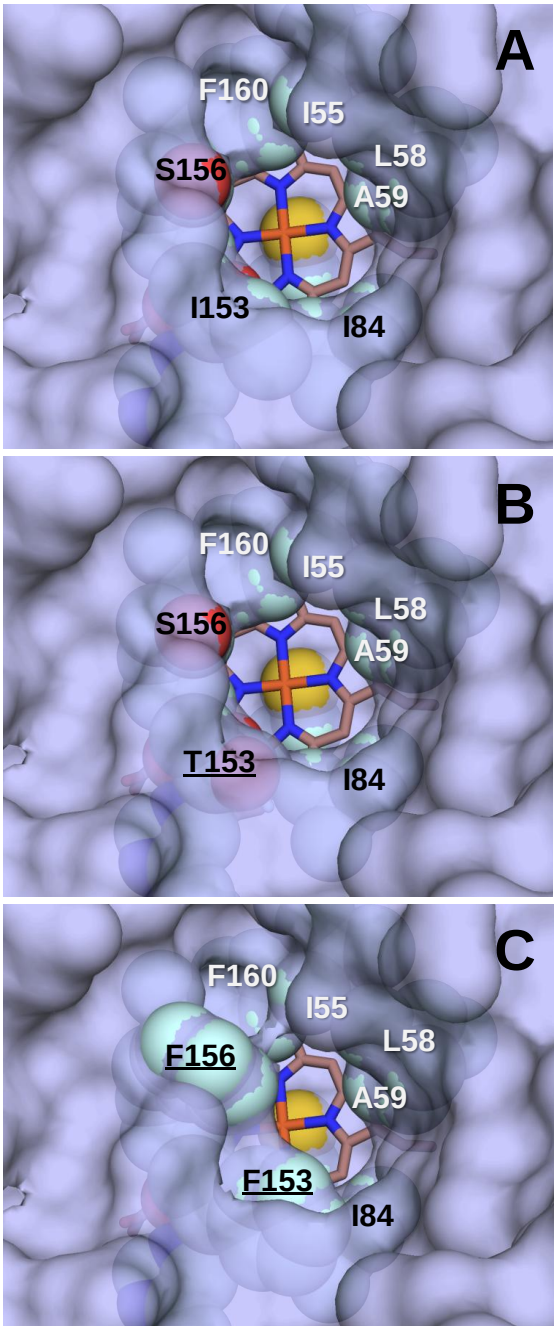

Figure S6. Comparison of the heme access channels of *Mro*UPO (**A**) and its I153T (**B**) and I153F/S156F (**C**) variants after *in silico* mutagenesis. Semi-transparent solvent-access surface (gray) and channel edge residues (CPK-colored spheres) are shown (with mutated residues underlined).

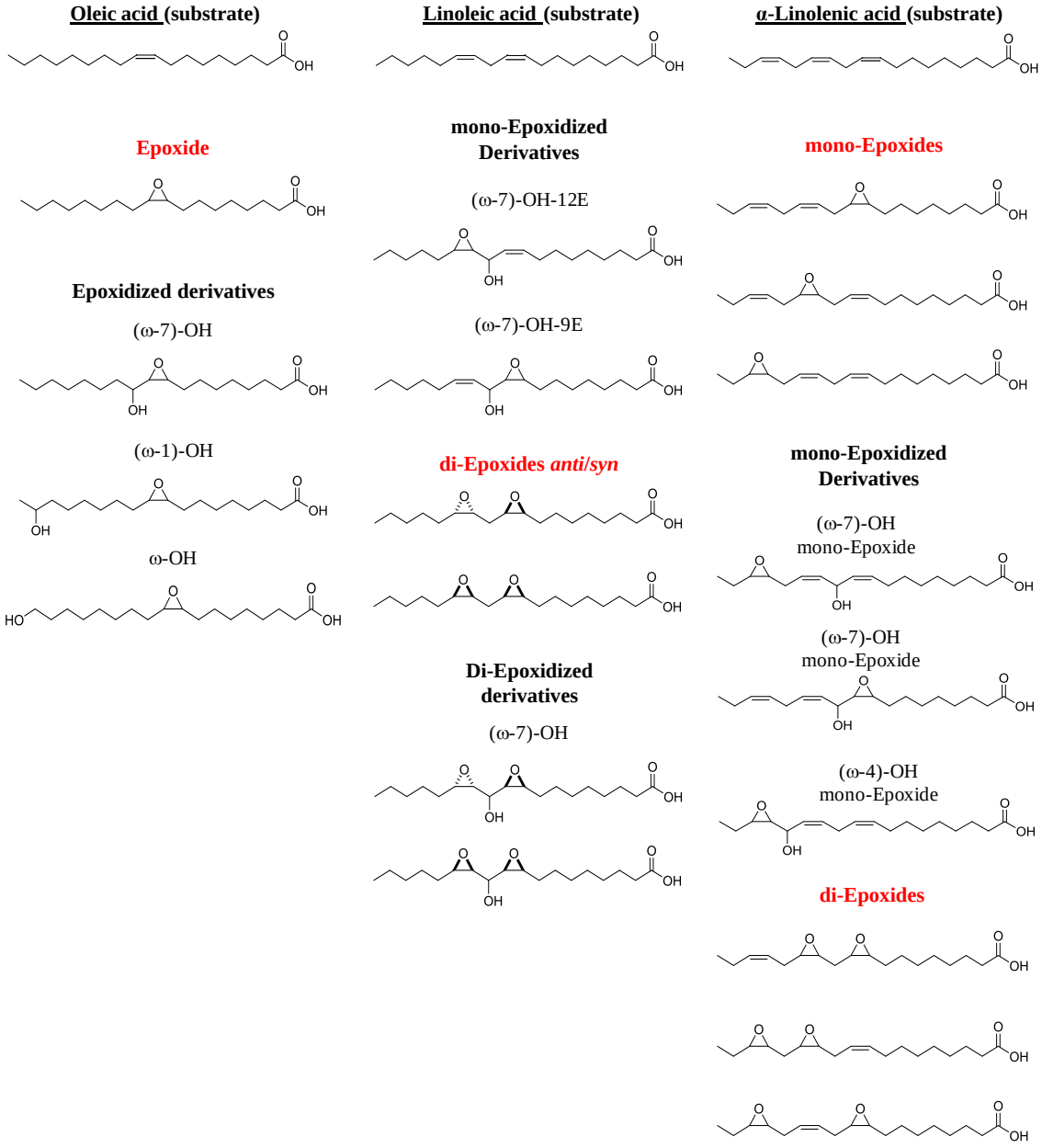

Figure S7. Formulae of epoxidized derivatives identified in the oleic (*left*), linoleic (*center*) and α-linolenic (*right*) acid reactions with *Mro*UPO and its I153T variant analyzed in **Figures 5** and **8**.

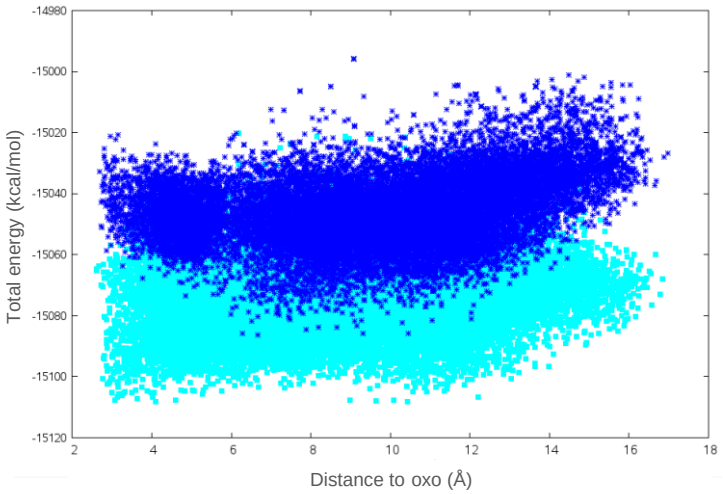

Figure S8. PELE migration of oleic acid for the *Mro*UPO (*blue*) and its I153T variant (*cyan*). The axis-x depicts the distance between the C-I oxo group and the C_{10} atom. Notice the (irrelevant) shift in total energies between both species due to the mutation. Therefore, analysis should involve only relative changes within one species.

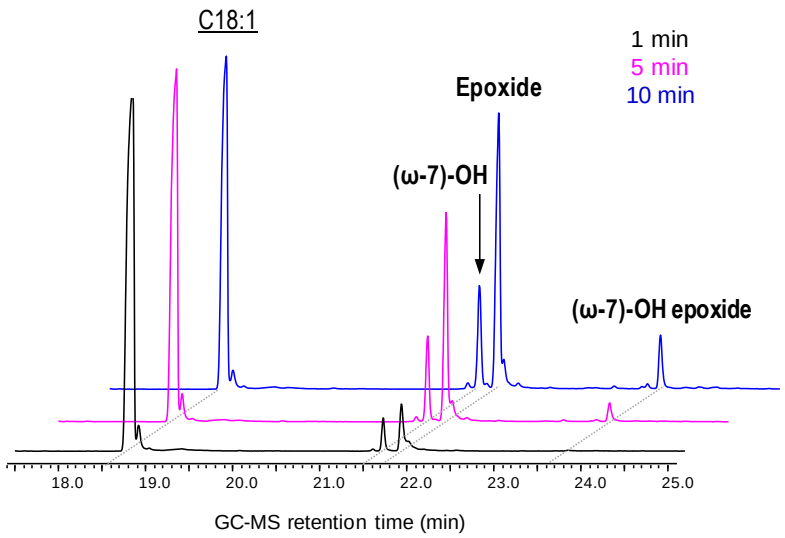

Figure S9. Initial (1-10 min) time course of oleic acid (C18:1, underlined) reactions with the I153T variant analyzed by GC-MS, showing simple epoxide (epoxidized oleic acid= 9,10-epoxystearic acid), (ω-7)-hydroxylated derivative, and double (ω-7)-hydroxylated and epoxidized derivative.

Supporting Material and Methods

- Heme C-I parameters:

Parameters were extracted from a QM/MM geometry optimization (20 steps) as described in the main text, with charges derived from the default Qsite ESP fitting. **Figure S10** shows the total spin density, clearly pointing to the two electrons ion the iron-oxo moiety, plus the porphyrin cation radical (with hydrogen atoms omitted for clarity).

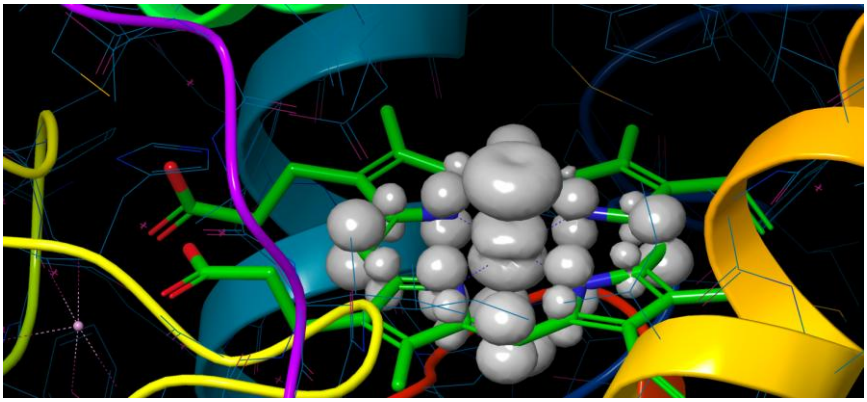

Figure S10. Total spin density in the heme C-I.

The parameter file that PELE uses is in IMPACT formatting. The first section shows the internal connection matrix. The NBON section illustrates the non-bonding terms, with QM/MM charges being the 4th field. Then, all bonding terms can be found.

```
* LIGAND DATABASE FILE (OPLS2005)
*
HEM      74    81    146    224     389
    1     0 S   CA    _CHA     1    16.80244    71.87270  -162.08939
    2     1 S   HA    _HHA    45     1.08395   133.48742    45.81616
    3     1 S   CW    _C1A     5     1.40374    16.93927    59.91474
    4     1 S   CW    _C4D    32     1.38867   109.53271  -130.77616
    5     3 S   CS    _C2A     6     1.45974   123.68346  -167.58320
    6     4 S   NB    _ND_    42     1.37827   122.96961    -0.28186
    7     5 S   CS    _C3A     7     1.36892   105.82407  -177.50739
    8     5 S   CT    _CAA    10     1.49766   124.23725     4.51492
    9     6 S   CW    _C1D    29     1.36726   105.08126  -178.17479
   10    37 S   Fe    FE__    43     2.00398   127.87950    -9.32799
   11    10 S   O     _O__    44     1.63448    93.18085   -86.83564
   12     8 S   HC    HAA1    52     1.09426   108.77834   163.18609
   13     8 S   HC    HAA2    53     1.09513   110.41399    48.02066
   14     9 S   CA    _CHD     4     1.39771   124.36852  -179.30959
   15    14 S   HA    _HHD    48     1.08439   116.54249   179.08550
   16     7 S   CW    _C4A     8     1.45170   106.62023     0.29074
   17     7 S   CT    _CMA     9     1.49621   128.88420  -178.49208
   18    17 S   HC    HMA1    49     1.09558   111.27110   139.68106
   19    17 S   HC    HMA2    50     1.09786   111.70533   -99.14264
   20    17 S   HC    HMA3    51     1.09207   110.56365    21.13932
   21     8 S   CT    _CBA    11     1.54226   116.17790   -73.09003
   22    21 S   HC    HBA1    54     1.09875   111.05803    40.53416
   23    21 S   HC    HBA2    55     1.09576   111.26505   -76.46592
   24     9 S   CS    _C2D    30     1.46129   111.06802     0.66852
   25    10 S   NB    _NC_    41     2.01259   176.78777    89.20254
   26    16 S   CA    _CHB     2     1.38147   124.15793   178.58805
   27    21 S   CO3   _CGA    12     1.55828   112.58703   160.33542
   28    27 S   O2Z   _O1A    13     1.26684   115.88597   167.64299
   29    27 S   O2Z   _O2A    14     1.25241   117.41678   -14.02355
   30    26 S   HA    _HHB    46     1.08455   116.13723    -1.33149
   31    25 S   CW    _C1C    22     1.37020   126.13489   109.11618
   32     4 S   CS    _C3D    31     1.46884   125.09314  -177.94729
   33    24 S   CT    _CMD    33     1.49716   123.79917   177.26248
   34    33 S   HC    HMD1    68     1.09066   111.77210   162.10470
   35    33 S   HC    HMD2    69     1.09621   111.78365   -77.34364
   36    33 S   HC    HMD3    70     1.09226   111.41908    41.65792
   37     3 S   NB    _NA_    39     1.36076   124.96165    14.48855
   38    26 S   CW    _C1B    15     1.40302   127.14380   175.99880
   39    31 S   CS    _C2C    23     1.44933   110.86391   170.15969
   40    32 S   CT    _CAD    34     1.52980   126.90342     4.30575
   41    40 S   HC    HAD1    71     1.09503   107.64304   158.01814
   42    40 S   HC    HAD2    72     1.09660   107.44013    44.02632
   43    38 S   CS    _C2B    16     1.44267   125.33766  -177.34134
   44    39 S   CS    _C3C    24     1.37416   106.17194     3.72063
```

```
45    39 S   CT   _CMC    26     1.49799   124.17929  -172.71358
46    45 S   HC   HMC1    62     1.09020   111.77788  -166.03500
47    45 S   HC   HMC2    63     1.09385   111.47170   -45.08416
48    45 S   HC   HMC3    64     1.09893   110.89308    73.49697
49    40 S   CT   _CBD    35     1.55797   117.06888   -78.74029
50    49 S   HC   HBD1    73     1.09071   108.94821    49.98196
51    49 S   HC   HBD2    74     1.09693   108.71716   -65.21913
52    43 S   CS   _C3B    17     1.38185   106.33163   175.97713
53    43 S   CT   _CMB    19     1.50065   127.50476    -5.75919
54    25 S   CW   _C4C    25     1.35937   127.10773   -80.84277
55    44 S   CM   _CAC    27     1.46337   130.12161   176.44929
56    49 S   CO3  _CGD    36     1.56761   120.26827   167.64426
57    56 S   O2Z  _O1D    37     1.31010   119.49476    61.26710
58    56 S   O2Z  _O2D    38     1.21624   115.80060  -122.54125
59    53 S   HC   HMB1    56     1.09680   110.77859   130.41805
60    53 S   HC   HMB2    57     1.09833   112.24582  -110.36144
61    53 S   HC   HMB3    58     1.09370   112.44462    10.45606
62    55 S   HC   _HAC    65     1.08669   115.84924   142.10411
63    52 S   CW   _C4B    18     1.45215   105.92408    -1.03703
64    52 S   CM   _CAB    20     1.46098   124.92465   178.97512
65    64 S   HC   _HAB    59     1.09151   114.37255    33.19899
66    55 S   CM   _CBC    28     1.33890   126.60679   -39.99030
67    66 S   HC   HBC1    66     1.08363   120.65700   179.56344
68    66 S   HC   HBC2    67     1.08613   122.66215    -0.75355
69    63 S   CA   _CHC     3     1.39532   125.54556  -173.23102
70    69 S   HA   _HHC    47     1.08405   116.32423     3.43878
71    64 S   CM   _CBB    21     1.34304   128.23772  -144.37786
72    71 S   HC   HBB1    60     1.08722   120.98142  -179.30733
73    71 S   HC   HBB2    61     1.08555   122.60626    -0.12195
74    10 S   NB   _NB_    40     2.04717    90.65924  -177.87551
14   6  14  13  16   9  14  11  13  18   1   5   4  10   4  10
 5   2   1   1   5   4   3  10   9   8   2   1   1   4  13  11
 4   2   1   1   1  10  12   8   5   4  11  11   6   2   1   1
 5   4   3  13   6   4   4   2   1   1   2   1   1   3   6   6
 3   2   1   1   2   1   2   1   1   1
 3     5     7    16     8     9    24    32     4    40    37     6    10     2
 3     4     5     6    32    37
 5     7    16    17     8    21    32     4    37     6    10    12    13    26
33    40    49    37     6    10    41    42     5     9    14    24    32
 7    16    17     8    21    27    37    10    18    19    20    12    13    22    23    26
10    15     9    14    24    32    33    40    54
16    17     8    21    38    37    10    30    18    19    20    12    13    26
21    27    28    29    37    12    13    22    23    16    17
24    32    33    40    25    10    15    34    35    36    14    44    54
11    14    16    24    25    26    31    32    37    38    39    43    44    52    54    63    69    74
 0
13    22    23    21    27
22    23    21    27
31    39    44    54    55    24    32    33    25    15
24    25    44    54
17    38    43    37    74    30    18    19    20    26
37    18    19    20    26
19    20
20
 0
27    28    29    22    23
23    27    28    29
27    28    29
32    33    40    49    34    35    36    41    42    54
70    31    39    44    45    54    55    63    69
38    43    52    63    53    37    74    30
28    29
29
 0
37    38    43    74
39    44    54    45    55    74    70    46    47    48    52    63    69
33    40    49    56    34    35    36    41    42    50    51
40    34    35    36
35    36
36
 0
38
43    52    63    53    64    74    59    60    61    69
44    54    45    55    66    70    46    47    48    62    63    69
49    56    57    58    41    42    50    51
42    50    51    49    56
50    51    49    56
52    63    53    64    71    74    59    60    61    65    69
54    45    55    66    46    47    48    62    67    68    69
55    46    47    48    54    69
47    48
48
 0
56    57    58    50    51
51    56    57    58
56    57    58
63    53    64    71    74    70    59    60    61    65    72    73    69
64    74    59    60    61    63
55    66    62    69
66    62    67    68
57    58
58
 0
60    61
61
 0
67    68    66
64    71    74    70    65    69
71    74    65    72    73    69
72    73    71
67    68
68
 0
```

```
   74    70
   74
   72    73
   73
    0
    0
NBON
    1   3.5500   0.0760  -0.207430   2.5000   1.7750   0.001000000  -0.843144165
    2   2.4200   0.0300   0.171670   1.3810   1.2100   0.030040813   0.268726247
    3   3.5500   0.0700   0.163560   2.5000   1.7750   0.001000000  -0.843144165
    4   3.5500   0.0700   0.477420   2.5000   1.7750   0.001000000  -0.843144165
    5   3.5500   0.0700  -0.111870   2.5000   1.7750   0.001000000  -0.843144165
    6   3.2500   0.1700  -0.491350   1.8650   1.6500   0.001000000  -0.511443539
    7   3.5500   0.0700   0.272610   2.5000   1.7750   0.001000000  -0.843144165
    8   3.5000   0.0660  -0.111420   1.9750   1.7500   0.005000000  -0.741685710
    9   3.5500   0.0700   0.306400   2.5000   1.7750   0.001000000  -0.843144165
   10   2.5940   0.0130   1.141360   1.4767   1.2970   0.005000000   0.000000000
   11   3.0000   0.1700  -0.495100   1.7000   1.5000   0.001000000  -0.126889456
   12   2.5000   0.0300   0.052080   1.4250   1.2500   0.008598240   0.268726247
   13   2.5000   0.0300   0.077560   1.4250   1.2500   0.008598240   0.268726247
   14   3.5500   0.0760  -0.246820   2.5000   1.7750   0.001000000  -0.843144165
   15   2.4200   0.0300   0.139700   1.3810   1.2100   0.030040813   0.268726247
   16   3.5500   0.0700  -0.050880   2.5000   1.7750   0.001000000  -0.843144165
   17   3.5000   0.0660  -0.493300   1.9750   1.7500   0.005000000  -0.741685710
   18   2.5000   0.0300   0.128200   1.4250   1.2500   0.008598240   0.268726247
   19   2.5000   0.0300   0.110470   1.4250   1.2500   0.008598240   0.268726247
   20   2.5000   0.0300   0.162980   1.4250   1.2500   0.008598240   0.268726247
   21   3.5000   0.0660  -0.136850   1.9750   1.7500   0.005000000  -0.741685710
   22   2.5000   0.0300   0.034350   1.3810   1.2100   0.008598240   0.268726247
   23   2.5000   0.0300   0.047220   1.3810   1.2100   0.008598240   0.268726247
   24   3.5500   0.0700   0.155390   2.5000   1.7750   0.001000000  -0.843144165
   25   3.2500   0.1700  -0.268610   1.8375   1.6250   0.005000000   0.000000000
   26   3.5500   0.0760  -0.121640   2.5000   1.7750   0.001000000  -0.843144165
   27   3.7500   0.1050   0.696030   2.1120   1.8750   0.001000000  -0.126889456
   28   2.9600   0.2100  -0.830450   1.7000   1.5000   0.001000000  -0.126889456
   29   2.9600   0.2100  -0.707730   1.7000   1.5000   0.001000000  -0.126889456
   30   2.4200   0.0300   0.134850   1.3810   1.2100   0.030040813   0.268726247
   31   3.5500   0.0700   0.001390   2.5000   1.7750   0.001000000  -0.843144165
   32   3.5500   0.0700  -0.652100   2.5000   1.7750   0.001000000  -0.843144165
   33   3.5000   0.0660  -0.324800   1.9750   1.7500   0.005000000  -0.741685710
   34   2.5000   0.0300   0.109140   1.4250   1.2500   0.008598240   0.268726247
   35   2.5000   0.0300   0.102850   1.4250   1.2500   0.008598240   0.268726247
   36   2.5000   0.0300   0.120820   1.4250   1.2500   0.008598240   0.268726247
   37   3.2500   0.1700  -0.320230   1.8375   1.6250   0.005000000   0.000000000
   38   3.5500   0.0700   0.002900   2.5000   1.7750   0.001000000  -0.843144165
   39   3.5500   0.0700   0.173080   2.5000   1.7750   0.001000000  -0.843144165
   40   3.5000   0.0660   0.536320   1.9750   1.7500   0.005000000  -0.741685710
   41   2.5000   0.0300  -0.002970   1.4250   1.2500   0.008598240   0.268726247
   42   2.5000   0.0300  -0.105840   1.4250   1.2500   0.008598240   0.268726247
   43   3.5500   0.0700   0.095940   2.5000   1.7750   0.001000000  -0.843144165
   44   3.5500   0.0700  -0.145600   2.5000   1.7750   0.001000000  -0.843144165
   45   3.5000   0.0660  -0.328060   1.9750   1.7500   0.005000000  -0.741685710
   46   2.5000   0.0300   0.101850   1.4250   1.2500   0.008598240   0.268726247
   47   2.5000   0.0300   0.074350   1.4250   1.2500   0.008598240   0.268726247
   48   2.5000   0.0300   0.106170   1.4250   1.2500   0.008598240   0.268726247
   49   3.5000   0.0660   0.539590   1.9750   1.7500   0.005000000  -0.741685710
   50   2.5000   0.0300  -0.174360   1.3810   1.2100   0.008598240   0.268726247
   51   2.5000   0.0300  -0.122500   1.3810   1.2100   0.008598240   0.268726247
   52   3.5500   0.0700  -0.093000   2.5000   1.7750   0.001000000  -0.843144165
   53   3.5000   0.0660  -0.330440   1.9750   1.7500   0.005000000  -0.741685710
   54   3.5500   0.0700   0.240760   2.5000   1.7750   0.001000000  -0.843144165
   55   3.5500   0.0760  -0.021780   2.0020   1.7750   0.023028004  -0.852763146
   56   3.7500   0.1050   0.659710   2.1120   1.8750   0.001000000  -0.126889456
   57   2.9600   0.2100  -1.278660   1.7000   1.5000   0.001000000  -0.126889456
   58   2.9600   0.2100  -0.616200   1.7000   1.5000   0.001000000  -0.126889456
   59   2.5000   0.0300   0.111400   1.4250   1.2500   0.008598240   0.268726247
   60   2.5000   0.0300   0.084030   1.4250   1.2500   0.008598240   0.268726247
   61   2.5000   0.0300   0.089350   1.4250   1.2500   0.008598240   0.268726247
   62   2.4200   0.0300   0.122870   1.4250   1.2500   0.008598240   0.268726247
   63   3.5500   0.0700   0.118020   2.5000   1.7750   0.001000000  -0.843144165
   64   3.5500   0.0760  -0.020390   2.0020   1.7750   0.023028004  -0.852763146
   65   2.4200   0.0300   0.114470   1.4250   1.2500   0.008598240   0.268726247
   66   3.5500   0.0760  -0.404700   2.0020   1.7750   0.023028004  -0.852763146
   67   2.4200   0.0300   0.181010   1.4250   1.2500   0.008598240   0.268726247
   68   2.4200   0.0300   0.165310   1.4250   1.2500   0.008598240   0.268726247
   69   3.5500   0.0760  -0.170150   2.5000   1.7750   0.001000000  -0.843144165
   70   2.4200   0.0300   0.173490   1.3810   1.2100   0.030040813   0.268726247
   71   3.5500   0.0760  -0.467320   2.0020   1.7750   0.023028004  -0.852763146
   72   2.4200   0.0300   0.159660   1.4250   1.2500   0.008598240   0.268726247
   73   2.4200   0.0300   0.173090   1.4250   1.2500   0.008598240   0.268726247
   74   3.2500   0.1700  -0.103510   1.8650   1.6500   0.001000000  -0.511443539
BOND
    1     3   469.000  1.400
    1     4   469.000  1.400
    1     2   367.000  1.080
   26    16   469.000  1.400
   26    38   469.000  1.400
   26    30   367.000  1.080
   69    63   469.000  1.400
   69    31   469.000  1.400
   69    70   367.000  1.080
   14    54   469.000  1.400
   14     9   469.000  1.400
   14    15   367.000  1.080
    3     5   469.000  1.400
    3    37   483.000  1.339
    5     7   469.000  1.400
    5     8   317.000  1.510
    7    16   469.000  1.400
    7    17   317.000  1.510
   16    37   483.000  1.339
   17    18   340.000  1.090
   17    19   340.000  1.090
```

17	20	340.000	1.090
8	21	268.000	1.529
8	12	340.000	1.090
8	13	340.000	1.090
21	27	317.000	1.522
21	22	340.000	1.090
21	23	340.000	1.090
27	28	656.000	1.250
27	29	656.000	1.250
38	43	469.000	1.400
38	74	483.000	1.339
43	52	469.000	1.400
43	53	317.000	1.510
52	63	469.000	1.400
52	64	320.000	1.460
63	74	483.000	1.339
53	59	340.000	1.090
53	60	340.000	1.090
53	61	340.000	1.090
64	71	549.000	1.340
64	65	340.000	1.080
71	72	340.000	1.080
71	73	340.000	1.080
31	39	469.000	1.400
31	25	483.000	1.339
39	44	469.000	1.400
39	45	317.000	1.510
44	54	469.000	1.400
44	55	320.000	1.460
54	25	483.000	1.339
45	46	340.000	1.090
45	47	340.000	1.090
45	48	340.000	1.090
55	66	549.000	1.340
55	62	340.000	1.080
66	67	340.000	1.080
66	68	340.000	1.080
9	24	469.000	1.400
9	6	483.000	1.339
24	32	469.000	1.400
24	33	317.000	1.510
32	4	469.000	1.400
32	40	317.000	1.510
4	6	483.000	1.339
33	34	340.000	1.090
33	35	340.000	1.090
33	36	340.000	1.090
40	49	268.000	1.529
40	41	340.000	1.090
40	42	340.000	1.090
49	56	317.000	1.522
49	50	340.000	1.090
49	51	340.000	1.090
56	57	656.000	1.250
56	58	656.000	1.250
37	10	300.000	2.004
74	10	300.000	2.047
25	10	300.000	2.013
6	10	300.000	2.036
10	11	300.000	1.634

THET

3	1	4	63.00000	120.00000
3	1	2	35.00000	120.00000
4	1	2	35.00000	120.00000
16	26	38	63.00000	120.00000
16	26	30	35.00000	120.00000
38	26	30	35.00000	120.00000
63	69	31	63.00000	120.00000
63	69	70	35.00000	120.00000
31	69	70	35.00000	120.00000
54	14	9	63.00000	120.00000
54	14	15	35.00000	120.00000
9	14	15	35.00000	120.00000
1	3	5	63.00000	120.00000
1	3	37	70.00000	124.00000
5	3	37	70.00000	124.00000
3	5	7	63.00000	120.00000
3	5	8	70.00000	120.00000
7	5	8	70.00000	120.00000
5	7	16	63.00000	120.00000
5	7	17	70.00000	120.00000
16	7	17	70.00000	120.00000
26	16	7	63.00000	120.00000
26	16	37	70.00000	124.00000
7	16	37	70.00000	124.00000
7	17	18	35.00000	109.50000
7	17	19	35.00000	109.50000
7	17	20	35.00000	109.50000
18	17	19	33.00000	107.80000
18	17	20	33.00000	107.80000
19	17	20	33.00000	107.80000
5	8	21	70.00000	112.17500
5	8	12	35.00000	109.50000
5	8	13	35.00000	109.50000
21	8	12	37.50000	110.70000
21	8	13	37.50000	110.70000
12	8	13	33.00000	107.80000
8	21	27	70.00000	109.69300
8	21	22	37.50000	110.70000
8	21	23	37.50000	110.70000
27	21	22	35.00000	109.50000
27	21	23	35.00000	109.50000
22	21	23	33.00000	107.80000

21	27	28	70.00000	117.00000
21	27	29	70.00000	117.00000
28	27	29	80.00000	126.00000
26	38	43	63.00000	120.00000
26	38	74	70.00000	124.00000
43	38	74	70.00000	124.00000
38	43	52	63.00000	120.00000
38	43	53	70.00000	120.00000
52	43	53	70.00000	120.00000
43	52	63	63.00000	120.00000
43	52	64	60.00000	120.93500
63	52	64	60.00000	120.93500
69	63	52	63.00000	120.00000
69	63	74	70.00000	124.00000
52	63	74	70.00000	124.00000
43	53	59	35.00000	109.50000
43	53	60	35.00000	109.50000
43	53	61	35.00000	109.50000
59	53	60	33.00000	107.80000
59	53	61	33.00000	107.80000
60	53	61	33.00000	107.80000
52	64	71	60.00000	123.20500
52	64	65	40.00000	117.26300
71	64	65	35.00000	120.00000
64	71	72	35.00000	120.00000
64	71	73	35.00000	120.00000
72	71	73	35.00000	117.00000
69	31	39	63.00000	120.00000
69	31	25	70.00000	124.00000
39	31	25	70.00000	124.00000
31	39	44	63.00000	120.00000
31	39	45	70.00000	120.00000
44	39	45	70.00000	120.00000
39	44	54	63.00000	120.00000
39	44	55	60.00000	120.93500
54	44	55	60.00000	120.93500
14	54	44	63.00000	120.00000
14	54	25	70.00000	124.00000
44	54	25	70.00000	124.00000
39	45	46	35.00000	109.50000
39	45	47	35.00000	109.50000
39	45	48	35.00000	109.50000
46	45	47	33.00000	107.80000
46	45	48	33.00000	107.80000
47	45	48	33.00000	107.80000
44	55	66	60.00000	123.20500
44	55	62	40.00000	117.26300
66	55	62	35.00000	120.00000
55	66	67	35.00000	120.00000
55	66	68	35.00000	120.00000
67	66	68	35.00000	117.00000
14	9	24	63.00000	120.00000
14	9	6	70.00000	124.00000
24	9	6	70.00000	124.00000
9	24	32	63.00000	120.00000
9	24	33	70.00000	120.00000
32	24	33	70.00000	120.00000
24	32	4	63.00000	120.00000
24	32	40	70.00000	120.00000
4	32	40	70.00000	120.00000
1	4	32	63.00000	120.00000
1	4	6	70.00000	124.00000
32	4	6	70.00000	124.00000
24	33	34	35.00000	109.50000
24	33	35	35.00000	109.50000
24	33	36	35.00000	109.50000
34	33	35	33.00000	107.80000
34	33	36	33.00000	107.80000
35	33	36	33.00000	107.80000
32	40	49	70.00000	112.17500
32	40	41	35.00000	109.50000
32	40	42	35.00000	109.50000
49	40	41	37.50000	110.70000
49	40	42	37.50000	110.70000
41	40	42	33.00000	107.80000
40	49	56	70.00000	109.69300
40	49	50	37.50000	110.70000
40	49	51	37.50000	110.70000
56	49	50	35.00000	109.50000
56	49	51	35.00000	109.50000
50	49	51	33.00000	107.80000
49	56	57	70.00000	117.00000
49	56	58	70.00000	117.00000
57	56	58	80.00000	126.00000
3	37	16	70.00000	117.00000
10	37	3	60.00000	127.87950
10	37	16	60.00000	126.24368
38	74	63	70.00000	117.00000
10	74	38	60.00000	126.65676
10	74	63	60.00000	126.97596
31	25	54	70.00000	117.00000
10	25	31	60.00000	126.13491
10	25	54	60.00000	127.10771
9	6	4	70.00000	117.00000
10	6	9	60.00000	126.27059
10	6	4	60.00000	128.56108
37	10	74	60.00000	90.65925
37	10	6	60.00000	88.85434
37	10	11	60.00000	93.18085
74	10	25	60.00000	89.50546
74	10	11	60.00000	91.00149
25	10	6	60.00000	90.62602
25	10	11	60.00000	90.02368

```
    6    10    11    60.00000   95.37543
PHI
    4     1     3     5   3.62500 -1.0 2.0
    4     1     3    37   3.62500 -1.0 2.0
    2     1     3     5   3.62500 -1.0 2.0
    2     1     3    37   3.62500 -1.0 2.0
    3     1     4    32   3.62500 -1.0 2.0
    3     1     4     6   3.62500 -1.0 2.0
    2     1     4    32   3.62500 -1.0 2.0
    2     1     4     6   3.62500 -1.0 2.0
   38    26    16     7   3.62500 -1.0 2.0
   38    26    16    37   3.62500 -1.0 2.0
   30    26    16     7   3.62500 -1.0 2.0
   30    26    16    37   3.62500 -1.0 2.0
   16    26    38    43   3.62500 -1.0 2.0
   16    26    38    74   3.62500 -1.0 2.0
   30    26    38    43   3.62500 -1.0 2.0
   30    26    38    74   3.62500 -1.0 2.0
   31    69    63    52   3.62500 -1.0 2.0
   31    69    63    74   3.62500 -1.0 2.0
   70    69    63    52   3.62500 -1.0 2.0
   70    69    63    74   3.62500 -1.0 2.0
   63    69    31    39   3.62500 -1.0 2.0
   63    69    31    25   3.62500 -1.0 2.0
   70    69    31    39   3.62500 -1.0 2.0
   70    69    31    25   3.62500 -1.0 2.0
    9    14    54    44   3.62500 -1.0 2.0
    9    14    54    25   3.62500 -1.0 2.0
   15    14    54    44   3.62500 -1.0 2.0
   15    14    54    25   3.62500 -1.0 2.0
   54    14     9    24   3.62500 -1.0 2.0
   54    14     9     6   3.62500 -1.0 2.0
   15    14     9    24   3.62500 -1.0 2.0
   15    14     9     6   3.62500 -1.0 2.0
    1     3     5     7   3.62500 -1.0 2.0
    1     3     5     8   3.62500 -1.0 2.0
   37     3    -5     7   3.62500 -1.0 2.0
   37     3     5     8   3.62500 -1.0 2.0
    1     3    37    16   3.62500 -1.0 2.0
    1     3    37    10   1.00000 -1.0 2.0
    5     3   -37    16   3.62500 -1.0 2.0
    5     3    37    10   1.00000 -1.0 2.0
    3     5    -7    16   3.62500 -1.0 2.0
    3     5     7    17   3.62500 -1.0 2.0
    8     5     7    16   3.62500 -1.0 2.0
    8     5     7    17   3.62500 -1.0 2.0
    3     5     8    21   0.04150 -1.0 2.0
    3     5     8    12   0.00000  1.0 1.0
    3     5     8    13   0.00000  1.0 1.0
    7     5     8    21   0.04150 -1.0 2.0
    7     5     8    12   0.00000  1.0 1.0
    7     5     8    13   0.00000  1.0 1.0
    5     7    16    26   3.62500 -1.0 2.0
    5     7   -16    37   3.62500 -1.0 2.0
   17     7    16    26   3.62500 -1.0 2.0
   17     7    16    37   3.62500 -1.0 2.0
    5     7    17    18   0.00000  1.0 1.0
    5     7    17    19   0.00000  1.0 1.0
    5     7    17    20   0.00000  1.0 1.0
   16     7    17    18   0.00000  1.0 1.0
   16     7    17    19   0.00000  1.0 1.0
   16     7    17    20   0.00000  1.0 1.0
   26    16    37     3   3.62500 -1.0 2.0
   26    16    37    10   1.00000 -1.0 2.0
    7    16   -37     3   3.62500 -1.0 2.0
    7    16    37    10   1.00000 -1.0 2.0
    5     8    21    27  -2.95950  1.0 1.0
    5     8    21    27   0.02300  1.0 3.0
    5     8    21    22   0.43200  1.0 3.0
    5     8    21    23   0.43200  1.0 3.0
   12     8    21    27  -0.11250  1.0 3.0
   12     8    21    22   0.15000  1.0 3.0
   12     8    21    23   0.15000  1.0 3.0
   13     8    21    27  -0.11250  1.0 3.0
   13     8    21    22   0.15000  1.0 3.0
   13     8    21    23   0.15000  1.0 3.0
    8    21    27    28   0.41150 -1.0 2.0
    8    21    27    29   0.41150 -1.0 2.0
   22    21    27    28   0.00000  1.0 1.0
   22    21    27    29   0.00000  1.0 1.0
   23    21    27    28   0.00000  1.0 1.0
   23    21    27    29   0.00000  1.0 1.0
   26    38    43    52   3.62500 -1.0 2.0
   26    38    43    53   3.62500 -1.0 2.0
   74    38   -43    52   3.62500 -1.0 2.0
   74    38    43    53   3.62500 -1.0 2.0
   26    38    74    63   3.62500 -1.0 2.0
   26    38   -74    10   1.00000 -1.0 2.0
   43    38   -74    63   3.62500 -1.0 2.0
   43    38    74    10   1.00000 -1.0 2.0
   38    43   -52    63   3.62500 -1.0 2.0
   38    43    52    64   3.62500 -1.0 2.0
   53    43    52    63   3.62500 -1.0 2.0
   53    43    52    64   3.62500 -1.0 2.0
   38    43    53    59   0.00000  1.0 1.0
   38    43    53    60   0.00000  1.0 1.0
   38    43    53    61   0.00000  1.0 1.0
   52    43    53    59   0.00000  1.0 1.0
   52    43    53    60   0.00000  1.0 1.0
   52    43    53    61   0.00000  1.0 1.0
   43    52    63    69   3.62500 -1.0 2.0
   43    52   -63    74   3.62500 -1.0 2.0
   64    52    63    69   3.62500 -1.0 2.0
```

64	52	63	74	3.62500	-1.0	2.0
43	52	64	71	0.15800	1.0	1.0
43	52	64	71	1.85350	-1.0	2.0
43	52	64	71	-0.48700	1.0	3.0
43	52	64	65	1.00000	-1.0	2.0
43	52	64	65	0.56550	1.0	3.0
63	52	64	71	0.15800	1.0	1.0
63	52	64	71	1.85350	-1.0	2.0
63	52	64	71	-0.48700	1.0	3.0
63	52	64	65	1.00000	-1.0	2.0
63	52	64	65	0.56550	1.0	3.0
69	63	74	38	3.62500	-1.0	2.0
69	63	74	10	1.00000	-1.0	2.0
52	63	-74	38	3.62500	-1.0	2.0
52	63	74	10	1.00000	-1.0	2.0
52	64	71	72	7.00000	-1.0	2.0
52	64	71	73	7.00000	-1.0	2.0
65	64	71	72	7.00000	-1.0	2.0
65	64	71	73	7.00000	-1.0	2.0
69	31	39	44	3.62500	-1.0	2.0
69	31	39	45	3.62500	-1.0	2.0
25	31	-39	44	3.62500	-1.0	2.0
25	31	39	45	3.62500	-1.0	2.0
69	31	25	54	3.62500	-1.0	2.0
69	31	-25	10	1.00000	-1.0	2.0
39	31	-25	54	3.62500	-1.0	2.0
39	31	25	10	1.00000	-1.0	2.0
31	39	-44	54	3.62500	-1.0	2.0
31	39	44	55	3.62500	-1.0	2.0
45	39	44	54	3.62500	-1.0	2.0
45	39	44	55	3.62500	-1.0	2.0
31	39	45	46	0.00000	1.0	1.0
31	39	45	47	0.00000	1.0	1.0
31	39	45	48	0.00000	1.0	1.0
44	39	45	46	0.00000	1.0	1.0
44	39	45	47	0.00000	1.0	1.0
44	39	45	48	0.00000	1.0	1.0
39	44	54	14	3.62500	-1.0	2.0
39	44	-54	25	3.62500	-1.0	2.0
55	44	54	14	3.62500	-1.0	2.0
55	44	54	25	3.62500	-1.0	2.0
39	44	55	66	0.15800	1.0	1.0
39	44	55	66	1.85350	-1.0	2.0
39	44	55	66	-0.48700	1.0	3.0
39	44	55	62	1.00000	-1.0	2.0
39	44	55	62	0.56550	1.0	3.0
54	44	55	66	0.15800	1.0	1.0
54	44	55	66	1.85350	-1.0	2.0
54	44	55	66	-0.48700	1.0	3.0
54	44	55	62	1.00000	-1.0	2.0
54	44	55	62	0.56550	1.0	3.0
14	54	25	31	3.62500	-1.0	2.0
14	54	25	10	1.00000	-1.0	2.0
44	54	-25	31	3.62500	-1.0	2.0
44	54	25	10	1.00000	-1.0	2.0
44	55	66	67	7.00000	-1.0	2.0
44	55	66	68	7.00000	-1.0	2.0
62	55	66	67	7.00000	-1.0	2.0
62	55	66	68	7.00000	-1.0	2.0
14	9	24	32	3.62500	-1.0	2.0
14	9	24	33	3.62500	-1.0	2.0
6	9	-24	32	3.62500	-1.0	2.0
6	9	24	33	3.62500	-1.0	2.0
14	9	6	4	3.62500	-1.0	2.0
14	9	-6	10	1.00000	-1.0	2.0
24	9	-6	4	3.62500	-1.0	2.0
24	9	6	10	1.00000	-1.0	2.0
9	24	-32	4	3.62500	-1.0	2.0
9	24	32	40	3.62500	-1.0	2.0
33	24	32	4	3.62500	-1.0	2.0
33	24	32	40	3.62500	-1.0	2.0
9	24	33	34	0.00000	1.0	1.0
9	24	33	35	0.00000	1.0	1.0
9	24	33	36	0.00000	1.0	1.0
32	24	33	34	0.00000	1.0	1.0
32	24	33	35	0.00000	1.0	1.0
32	24	33	36	0.00000	1.0	1.0
24	32	4	1	3.62500	-1.0	2.0
24	32	-4	6	3.62500	-1.0	2.0
40	32	4	1	3.62500	-1.0	2.0
40	32	4	6	3.62500	-1.0	2.0
24	32	40	49	0.04150	-1.0	2.0
24	32	40	41	0.00000	1.0	1.0
24	32	40	42	0.00000	1.0	1.0
4	32	40	49	0.04150	-1.0	2.0
4	32	40	41	0.00000	1.0	1.0
4	32	40	42	0.00000	1.0	1.0
1	4	6	9	3.62500	-1.0	2.0
1	4	-6	10	1.00000	-1.0	2.0
32	4	-6	9	3.62500	-1.0	2.0
32	4	6	10	1.00000	-1.0	2.0
32	40	49	56	-2.95950	1.0	1.0
32	40	49	56	0.02300	1.0	3.0
32	40	49	50	0.43200	1.0	3.0
32	40	49	51	0.43200	1.0	3.0
41	40	49	56	-0.11250	1.0	3.0
41	40	49	50	0.15000	1.0	3.0
41	40	49	51	0.15000	1.0	3.0
42	40	49	56	-0.11250	1.0	3.0
42	40	49	50	0.15000	1.0	3.0
42	40	49	51	0.15000	1.0	3.0
40	49	56	57	0.41150	-1.0	2.0
40	49	56	58	0.41150	-1.0	2.0

```
   50    49    56    57   0.00000  1.0 1.0
   50    49    56    58   0.00000  1.0 1.0
   51    49    56    57   0.00000  1.0 1.0
   51    49    56    58   0.00000  1.0 1.0
IPHI
    4     2     1     3   1.10000 -1.0 2.0
   38    30    26    16   1.10000 -1.0 2.0
   31    70    69    63   1.10000 -1.0 2.0
    9    15    14    54   1.10000 -1.0 2.0
    5    37     3     1   4.00000 -1.0 2.0
    7     8     5     3   4.00000 -1.0 2.0
   16    17     7     5   4.00000 -1.0 2.0
    7    37    16    26   4.00000 -1.0 2.0
   29    21    27    28  10.50000 -1.0 2.0
   43    74    38    26   4.00000 -1.0 2.0
   52    53    43    38   4.00000 -1.0 2.0
   63    64    52    43   4.00000 -1.0 2.0
   52    74    63    69   4.00000 -1.0 2.0
   52    65    64    71  15.00000 -1.0 2.0
   72    73    71    64  15.00000 -1.0 2.0
   39    25    31    69   4.00000 -1.0 2.0
   44    45    39    31   4.00000 -1.0 2.0
   54    55    44    39   4.00000 -1.0 2.0
   44    25    54    14   4.00000 -1.0 2.0
   44    62    55    66  15.00000 -1.0 2.0
   67    68    66    55  15.00000 -1.0 2.0
   24     6     9    14   4.00000 -1.0 2.0
   32    33    24     9   4.00000 -1.0 2.0
    4    40    32    24   4.00000 -1.0 2.0
   32     6     4     1   4.00000 -1.0 2.0
   58    49    56    57  10.50000 -1.0 2.0
   10    16    37     3   2.50000 -1.0 2.0
   10    63    74    38   2.50000 -1.0 2.0
   10    54    25    31   2.50000 -1.0 2.0
   10     4     6     9   2.50000 -1.0 2.0
END
```